Cell Reports

Article

Alpha-synuclein abundance and localization are regulated by the RNA-binding protein PUMILIO1

Graphical abstract

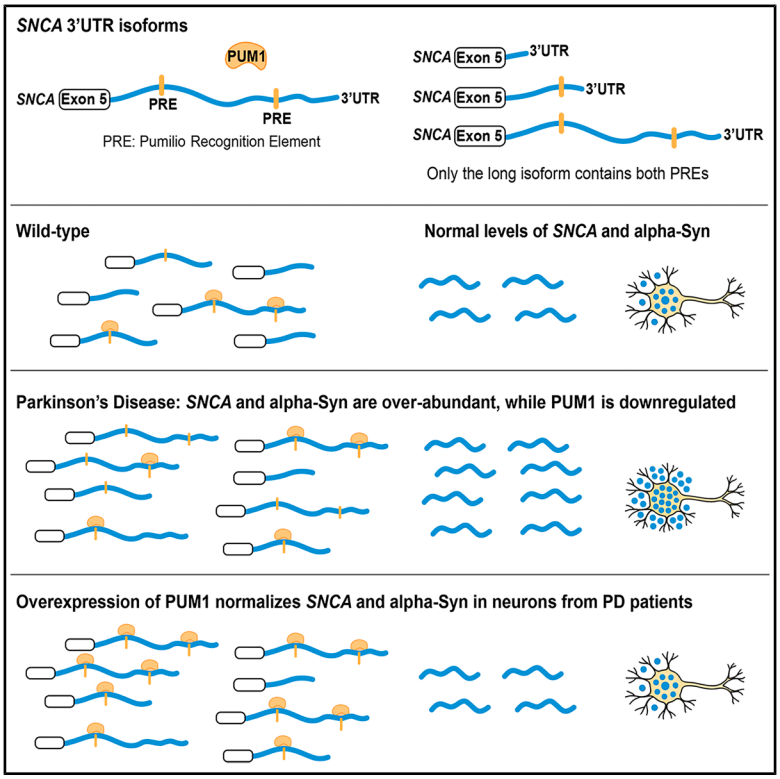

Highlights

- PUM1 binds two recognition elements at the 3′ UTR of *SNCA* mRNA in human cells
- PUM1 suppresses α-synuclein in dopaminergic cells vulnerable in Parkinson's disease (PD)
- PUM1 suppresses the long *SNCA* isoform, whose levels rise more in PD
- Some cases of PD involve *PUM1* variants that cannot bind the *SNCA* 3′ UTR

Authors

Maximilian Cabaj, Pietro G. Mazzara, Zachary A. Gaertner, ..., Ulrich Hengst, Rajeshwar Awatramani, Vincenzo A. Gennarino

Correspondence

vag2138@cumc.columbia.edu

In brief

Cabaj et al. find that the RNA-binding protein PUM1 regulates α-synuclein levels by binding two Pumilio recognition elements in the *SNCA* 3′ UTR in mice and human neurons. The long *SNCA* isoform, which contains both PUM1 recognition elements (PREs), is upregulated in Parkinson's disease and responsive to PUM1 suppression.

Cabaj et al., 2025, Cell Reports *44*, 116145
August 26, 2025 Published by Elsevier Inc.
https://doi.org/10.1016/j.celrep.2025.116145

CellPress

Cell Reports

CellPress
OPEN ACCESS

Article

Alpha-synuclein abundance and localization are regulated by the RNA-binding protein PUMILIO1

Maximilian Cabaj,[1] Pietro G. Mazzara,[1] Zachary A. Gaertner,[2] Ruizhi Wang,[3,4] Michaela M. Pauers,[3] Lisa K. Randolph,[5] Cláudio Gouveia Roque,[6] Sean Feeney,[5] Serena Raimo,[1] Nicola de Prisco,[1] Alexei Chemiakine,[1] Xinyuan Wang,[7,8] Ravi K. Singh,[9] Swetha Rajasekaran,[10,11] Hari K. Yalamanchili,[12,13] Wayne Miles,[10,11] Kristin Baldwin,[1] Chaolin Zhang,[14,15] Matthew B. Harms,[4] Vikram Khurana,[7,8,16,17] Vicky Brandt,[1] Ulrich Hengst,[3,6] Rajeshwar Awatramani,[2] and Vincenzo A. Gennarino[1,4,18,19,20,21,*]

[1]Department of Genetics and Development, Columbia University Irving Medical Center, New York, NY, USA
[2]Department of Neurology, Northwestern University, Chicago, IL, USA
[3]Department of Pathology and Cell Biology, Columbia University Vagelos College of Physicians and Surgeons, New York, NY, USA
[4]Department of Neurology, Columbia University Irving Medical Center, New York, NY, USA
[5]Doctoral Program in Neurobiology and Behavior, Columbia University, New York, NY, USA
[6]Taub Institute for Research on Alzheimer's Disease and the Aging Brain, Columbia University Vagelos College of Physicians and Surgeons, New York, NY, USA
[7]Division of Movement Disorders, American Parkinson Disease Association (APDA) Center for Advanced Research and MSA Center of Excellence, Department of Neurology, Brigham and Women's Hospital, Boston, MA, USA
[8]Harvard Stem Cell Institute, Cambridge, MA, USA
[9]Department of Pharmacological and Pharmaceutical Sciences, College of Pharmacy University of Houston, Houston, TX, USA
[10]Department of Cancer Biology and Genetics, The Ohio State University, 460 West 12th Avenue, Columbus, OH 43210, USA
[11]The Ohio State University Comprehensive Cancer Center, The Ohio State University, 460 West 12th Avenue, Columbus, OH 43210, USA
[12]Jan and Dan Duncan Neurological Research Institute, Texas Children's Hospital, Houston, TX, USA
[13]USDA/ARS Children's Nutrition Research Center, Department of Pediatrics, Baylor College of Medicine, Houston, TX, USA
[14]Department of Systems Biology, Columbia University Irving Medical Center, New York, NY, USA
[15]Department of Biochemistry and Molecular Biophysics, Columbia University Irving Medical Center, New York, NY, USA
[16]Harvard Medical School, Boston, MA, USA
[17]The Broad Institute of MIT and Harvard, Cambridge, MA, USA
[18]Department of Pediatrics, Columbia University Irving Medical Center, New York, NY, USA
[19]Columbia Stem Cell Initiative, Columbia University Irving Medical Center, New York, NY, USA
[20]Initiative for Columbia Ataxia and Tremor, Columbia University Irving Medical Center, New York, NY, USA
[21]Lead contact
*Correspondence: vag2138@cumc.columbia.edu
https://doi.org/10.1016/j.celrep.2025.116145

SUMMARY

The protein α-synuclein, encoded by *SNCA*, accumulates in Parkinson's disease (PD) and other synucleinopathies for reasons that remain unclear. Here, we investigated whether *SNCA* is regulated *in vivo* by the RNA-binding protein PUM1. We establish that PUM1 binds to *SNCA*'s 3′ UTR in mouse and human cells. In induced neurons from patients with *SNCA* locus triplication, *PUM1* mRNA levels are lower than in healthy controls, but increasing PUM1 normalizes both *SNCA* mRNA and α-synuclein protein levels, largely by suppressing the long 3′ UTR *SNCA* isoform. In microfluidic chamber experiments, silencing *PUM1* causes a redistribution of *SNCA* between the soma and axons. We also show that the previously described miR-7 regulation of *SNCA* mRNA requires PUM1. Lastly, we report finding several individuals with PD in clinical databases bearing variants in *PUM1* that affect its RNA-binding ability. Understanding how RNA-binding proteins regulate α-synuclein could lead to viable new therapies for synucleinopathies.

INTRODUCTION

Proteostasis is so crucial to neuronal function that its dysregulation underlies a number of neurodegenerative diseases. These "proteopathies," which include both familial and sporadic diseases such as Alzheimer's and Parkinson's, differ from each other in many respects but are all characterized pathologically by the abnormal accumulation of a disease-related protein in neurons. In inherited proteopathies such as Huntington's disease, a mutation alters the conformation of the disease-causing protein in such a way that it resists the neuron's usual mechanisms of protein clearance and eventually forms inclusions in neurons.[1] Even too

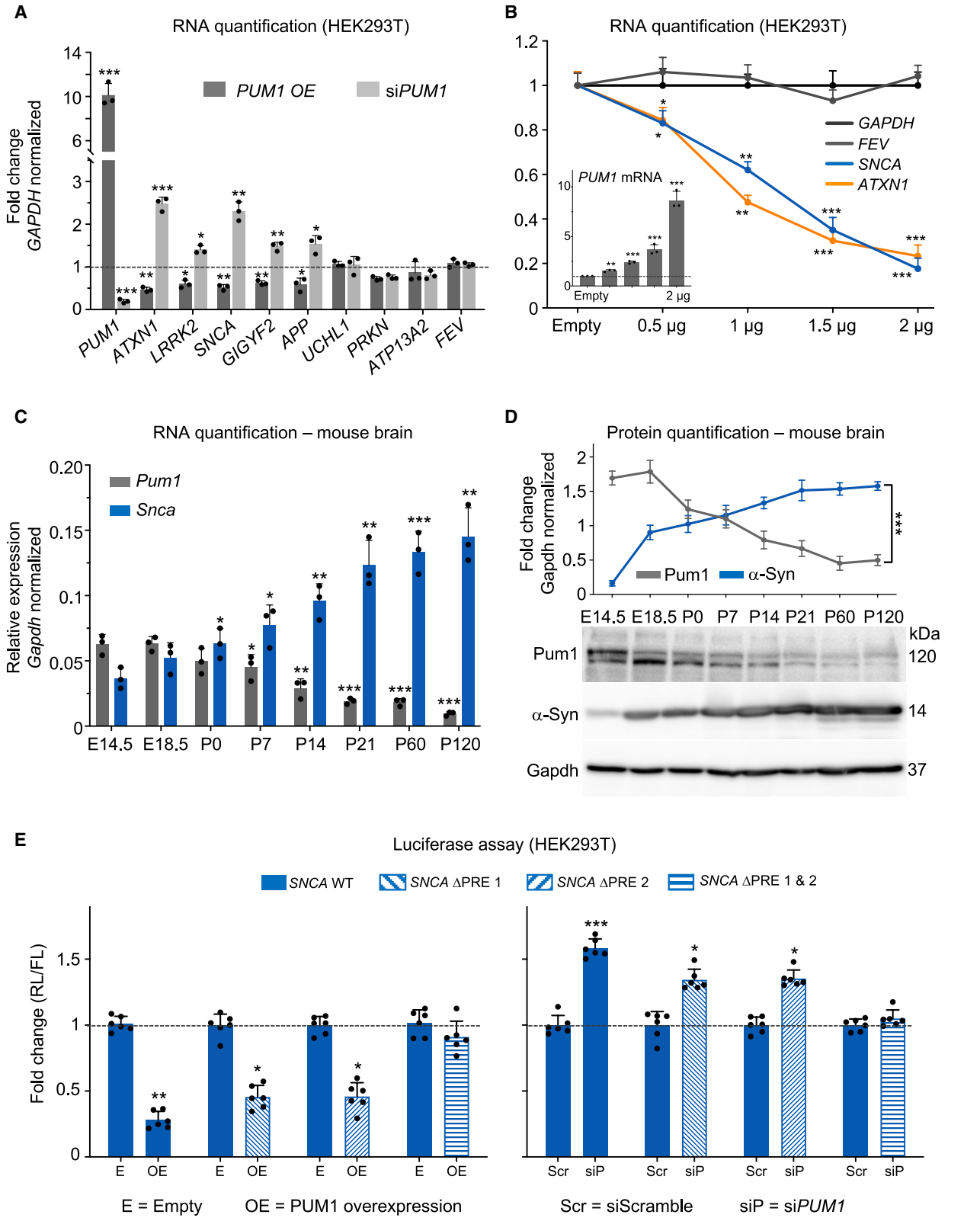

(legend on next page)

much wild-type (WT) protein can be neurotoxic, however: duplications or triplications of the *SNCA* locus cause overexpression of α-synuclein, leading to a familial Parkinson's disease (PD) whose severity correlates with gene dosage.[2] There has thus been considerable interest in therapeutic approaches that reduce the steady-state concentrations of neurodegenerative-disease-related proteins such as α-synuclein,[3] which is involved not just in PD but also in multiple system atrophy (MSA), Lewy body dementia, and neuroaxonal dystrophies, among others.[4,5] To reduce α-synuclein to physiological levels requires that we understand the variety of mechanisms by which it accumulates, and why it affects different cell types in different synucleinopathies.

For these reasons, several groups have sought to understand the endogenous pathways that regulate α-synuclein abundance. For example, RNA-binding proteins (RBPs) and microRNAs (miRNAs) commonly influence various aspects of RNA fate, including RNA localization and stability, by binding to the 3′ UTRs of target mRNAs. Indeed, several miRNAs—miR-7, miR-34b, miR-153, and miR-34c—have been found to influence α-synuclein abundance by binding the *SNCA* 3′ UTR,[6,7] at least in cellular systems, with more possibilities to be tested.[8] Of these, miR-7 and miR-153 together repress *SNCA* mRNA expression by ∼47% in experimental cell models and in the MPTP neurotoxin mouse model[7,9]; miR-7 seems to facilitate the degradation of α-synuclein, and loss of miR-7 in mice leads to accumulation of α-synuclein with associated nigral dopaminergic loss.[10,11] Intriguingly, miR-7 levels have been found to be lower than normal in the substantia nigra pars compacta (SNpc) of patients with PD.[11] The role of RBPs in the regulation of PD-linked genes has been less explored: to our knowledge, the first RBPs found to regulate *SNCA* were ELAVL1 and TIAR1, in 2017.[12] They increase the levels of *SNCA* mRNA (primarily the short isoform) by binding its 3′ UTR.[12] Interestingly, the authors note that TIAR1 is downregulated in PD while ELAVL1 is upregulated in MSA. More recently, the RBP AUF1 was shown to destabilize *SNCA* transcripts in the cytosol (again, predominantly the short isoforms) by inhibiting their association with ribosomes, thereby reducing α-synuclein levels.[13] It is also worth noting that although the short isoform is thought to contribute more to protein synthesis,[12] the long isoform seems to increase in PD.[14]

In the course of investigating the role of the RBP PUMILIO1 (PUM1) in neurological function in mice and humans,[15,16] we performed a genome-wide search for conserved PUM1 recognition elements (PREs) in 3′ UTRs and identified several genes associated with PD, including *SNCA*, as putative targets. PUM1 can repress translation of its targets by any of three mechanisms[17]: it can bind directly to the transcript's 3′ UTR at PREs, which consist of a well-conserved motif (UGUA[N]AUA) in the corresponding DNA[18]; it can recruit the CCR4-NOT deadenylase complex to inhibit translation or degrade the mRNA[19,20]; or it can cooperate with AGO2 to employ the miRNA machinery to repress translation. We therefore set out to determine whether *SNCA* mRNA is a genuine target of PUM1 and to understand the mechanisms of its regulation across multiple models, including mouse, rat, and neurons derived from patients with PD.

RESULTS

PUM1 binds PREs in the *SNCA* 3′ UTR in human cells and mouse brain

We performed a genome-wide bioinformatics analysis to identify all genes with at least one PRE in their 3′ UTR and found 4,279 unique putative mRNAs (Table S1). To narrow down the number of candidate targets, we focused on candidates with at least one PRE conserved between humans and mice in the 3′ UTRs. This resulted in 2,187 candidate targets, for which we performed Ingenuity Pathway Analysis (IPA).[21] We selected all categories with $-\log_{10}(p$ values) >3 and ranked them by statistical significance (Figure S1A and Table S2). "Developmental disorder" was the most enriched category (Figure S1A), but the second-highest ranked term, "neurological disease," had the largest number of targets. We further expanded this category and repeated the IPA to generate an enrichment network, identifying five subcategories (Parkinson's disease, Alzheimer's disease, tauopathy, bipolar disorder, and movement disorders) along with four PD-linked genes (*SNCA*, *LRRK2*, *APP*, and *GIGYF2*) (Figure S1B).

To assess the functional relationship between PUM1 and these four putative target mRNAs, we overexpressed or silenced *PUM1* in HEK293T cells and quantified the mRNA levels of *LRRK2*, *SNCA*, *GIGYF2*, and *APP*, using *ATXN1*[15,16] as a positive control. As negative controls, we included three PD-associated genes that do not contain PREs (*UCHL1*, *PRKN*, and *ATP13A2*)[22–24] and *FEV*, which neither contains a PRE nor is linked to PD. All genes without PREs were unaffected by PUM1 overexpression or knockdown. In contrast, the four predicted PD-linked mRNAs showed an inverse correlation to PUM1 expression: *SNCA* mRNA levels were most affected, being reduced by ∼50% following *PUM1* overexpression and increased by ∼150% following knockdown (Figure 1A). Neuroblastoma SH-SY5Y cell lines showed the same inverse correlation between PUM1 and the PD-associated genes, with *SNCA*

Figure 1. PUM1 regulates *SNCA* by binding to both PREs in its 3′ UTR and is inversely correlated with α-Syn expression during development

(A) qPCR of PD risk genes with or without a PRE in their 3′ UTR, after knockdown or overexpression of *PUM1* in HEK293T cells. *SNCA* showed the strongest response to changes in PUM1 expression. *ATXN1* was used as a positive control and *FEV* as a non-PD-related negative control. Data were normalized to *GAPDH* and then compared to cells treated with an empty vector for *PUM1* overexpression (OE) and siScramble for *PUM1* knockdown experiments.

(B) qPCR in HEK293T cells transfected with 0.5–2 μg of *PUM1*. Data were normalized to *GAPDH* and then compared to cells treated with an empty vector.

(C) qPCR of *Pum1* and *Snca* from brains of wild-type (WT) mice from gestation (embryonic day 14.5) to young adulthood (post-natal 120 days [P120]). Data were normalized to *Gapdh* mRNA levels.

(D) Representative western blot and relative quantification of Pum1 and α-Syn protein levels from E14.5 to P120, confirming their inverse relationship.

(E) Ratio of Renilla luciferase (RL) to firefly luciferase (FL) in HEK293T cells transfected with full-length *SNCA* 3′ UTR subcloned into the psiCHECK-2 vector, along with either overexpression (left) or silencing (right) of *PUM1* in the context of mutating PRE1, PRE2, or both. Empty vector and siScramble were used as negative controls for *PUM1* overexpression and silencing, respectively.

All data represent the mean ± SEM from at least three biological replicates (indicated here as single dots). Statistical significance was calculated using Student's t test: $^{*}p < 0.05$, $^{**}p < 0.01$, $^{***}p < 0.001$. See also Figure S1.

mRNA again being the most strongly affected (Figure S1C). Stepwise increases in PUM1 expression led to corresponding decreases in *SNCA* mRNA in HEK293T cells (Figure 1B). We decided to focus on *SNCA* because it showed the strongest response to PUM1 dysregulation in cells.

To examine the relationship between Pum1 and α-Syn in mice, we first measured their RNA and protein levels at various developmental time points in the mouse brain. The results show the same anti-correlation we observed in human cells (Figures 1C and 1D). (Here and throughout this paper, we will refer to the human genes and proteins in all uppercase, e.g., *SNCA*, but use an initial capital only, e.g., *Snca*, for murine genes and proteins).

To determine how PUM1 represses *SNCA* mRNA, we focused on its PREs. The canonical long human *SNCA* isoform has a 3′ UTR that is 2,529 nt long and contains two PREs[14]: the proximal site, located from 525 to 532 nt (PRE1), and the distal site, from 1,663 to 1,671 nt (PRE2) (Figure S1D) (there is also a more recently discovered, even longer isoform[25] as well as several possible shorter isoforms[14]; Figure S1D). We deleted either PRE1, PRE2, or both, and quantified *SNCA* using a luciferase assay after overexpression or silencing of *PUM1* (Figure 1E). *PUM1* overexpression suppressed *SNCA* expression ∼75%; deleting either the proximal or distal PRE relieved *SNCA* suppression, bringing it up to half WT levels, whereas deletion of both PREs restored *SNCA* expression (Figure 1E, left). Similarly, in the context of *PUM1* knockdown, deletion of both PREs protected *SNCA* transcripts from PUM1 suppression (Figure 1E, right). Thus, the two PREs have an additive effect in human cells.

The murine *Snca* 3′ UTR contains one conserved PRE (Figure S1D). We performed RNA crosslinking immunoprecipitation (RNA-CLIP)[15] on whole brains from 3-week-old WT mice, using *Pum1*-knockout (KO) mice as negative controls (Figure 2A). RNA-CLIP in WT mice confirmed a specific interaction between Pum1 and the conserved PRE within the *Snca*3′ UTR in the brain; as expected for a negative control, no enrichment was detected in *Pum1*-KO mice (Figure 2A). In a randomized, blinded assay, *Snca* mRNA levels increased by 40% in *Pum1*-Het mice and by 70% in *Pum1*-KO mice (Figure 2B), while α-Syn protein levels increased by 32% and 87%, respectively (Figures 2C and 2D). Therefore, Pum1 binds and negatively regulates *Snca* in the mouse brain.

Since PUM1's close homolog PUM2 also binds PREs[26] and co-regulates some of the same targets,[8] we asked whether PUM2 might also influence *SNCA*. In fact, a prior study in SH-SY5Y cells suggested that both PUM1 and PUM2 may regulate *SNCA*.[8] We manipulated *PUM2* in HEK293T cells and examined the effects on both *PUM1* and *SNCA* mRNA levels. Silencing *PUM2* led to an increase in *PUM1* levels and a concomitant decrease in *SNCA* mRNA. Conversely, *PUM2* overexpression reduced *PUM1* expression and increased *SNCA* levels (Figure 2E). These findings confirm that *SNCA* is directly regulated by PUM1 but that PUM2 could exert an indirect effect through its influence on PUM1 expression.

Pum1 suppresses *Snca* mRNA to different degrees in different mouse brain regions

We have previously shown that some Pum1 interactions vary across different brain regions while others remain constant.[27] To explore the relationship between *Pum1* and *Snca* mRNA in different brain regions, we performed quantitative *in situ* hybridization (ISH) with painted probes[15] against *Pum1* and *Snca* mRNAs in *Pum1*-Het and *Pum1*-KO mice. Signal intensity was scored along a gradient, from yellow (low) to blue (medium) and red (high), and quantified as a function of the number of colored pixels for each color and overall, compared to WT (see STAR Methods). We observed an overall 50% reduction in *Pum1*-Het and a very low signal in *Pum1*-KO brains in all three channels (Figure S2A).

ISH against *Snca* in whole-brain samples suggested no significant change in *Snca* transcripts overall with *Pum1* loss (Figure S2B). There were no appreciable changes in the low and medium channels, but the high-intensity channel showed higher levels of *Snca* transcripts in the context of *Pum1* haploinsufficiency or knockout (Figure S2B). This suggests a significant increase in *Snca* mRNA within the same neurons, rather than from new cells. *Snca* increased in the cortex, hippocampus, and SNpc to varying degrees with loss of *Pum1* (Figure 3A). Significant elevations were found in medium-signal (blue) and high-signal (red) foci in the hippocampus (Figure 3A). In the SNpc, global *Snca* levels were increased in *Pum1*-Het mice, with expression rising 250% compared to WT in the red channel, while in *Pum1*-KO, *Snca* increased by ∼300% (Figure 3A).

To evaluate the increase of *Snca* mRNA at single-neuron resolution in the SNpc, we performed RNAscope on brain sections from *Pum1*-Het and *Pum1*-KO mice compared to WT controls using a probe targeting tyrosine hydroxylase (*Th*) mRNA to mark dopaminergic neurons in the SNpc (Figures 3B, S3A, and S3B). *Snca* transcripts were proportionally elevated in both *Pum1*-Het and *Pum1*-KO mice. To test possible compensation by Pum2 in the SNpc, we measured *Pum2* mRNA expression across different brain regions using ISH. *Pum2* expression increased across many regions, particularly in the hippocampus and cerebellum, but was undetectable in the SNpc (Figures S3C and S4).

Pum1 influences *Snca* localization in specific neuronal compartments

In PD, α-Syn accumulates in the axon, impairing microtubule-based transport from the soma to the terminals.[28] Given that Pum2 retains target mRNAs in the soma during axonal development,[29] we wondered whether Pum1 might also influence the subcellular distribution of *Snca* mRNA. To this end, we transduced rat hippocampal neurons with either shPum1 or Pum1 overexpression (OE) viruses, and compared them to shControls and empty controls, respectively. We found that Pum1 OE in rat hippocampal neurons reduced *Snca* mRNA and α-Syn protein levels by approximately 50% and 70%, respectively (Figures 4A and 4B). Conversely, sh*Pum1* increased *Snca* mRNA and α-Syn protein levels.

To determine whether this regulation is compartment specific, we cultured rat hippocampal neurons in microfluidic chambers to isolate the soma from the axon[29] and treated the somatic compartment with shPum1. We then lysed the cells in a compartment-specific manner for qPCR. *Pum1* mRNA levels in the soma fell by ∼50% without significantly affecting axonal *Pum1*. This change, however, led to a

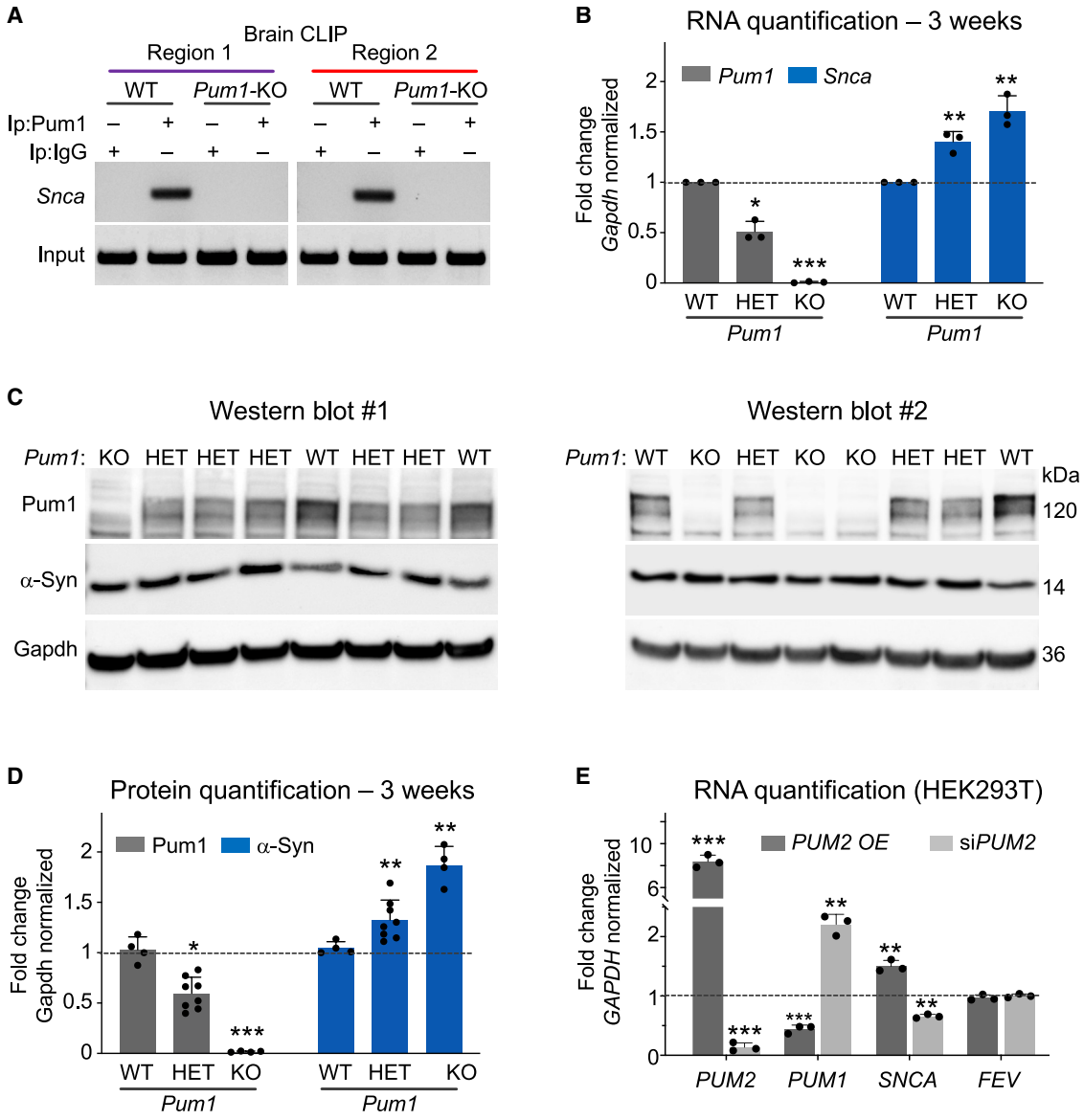

Figure 2. Pum1 regulates α-Syn protein and *Snca* mRNA levels in the mouse brain

(A) RNA-CLIP for the conserved *Snca* PRE, following immunoprecipitation (IP) against Pum1, in mouse brains at 3 weeks of age. The purple and red lines indicate PCR fragments upstream of the conserved *Snca* 3′ UTR PRE (508–515) (Figure S1D). IP against IgG and *Pum1*-KO mice were used as negative controls. RNA lysate from 10% of the pre-cleared lysate was used as input; see STAR Methods.

(B) RNA quantification by qPCR of *Pum1* and *Snca* from WT, *Pum1*-Het, and *Pum1*-KO mouse brains at 3 weeks of age. Data were normalized to *Gapdh* and represent means ± SEM from three biological replicates.

(C and D) (C) Randomized and blinded western blots and (D) quantification of Pum1 and α-Syn from *Pum1*-Het and -KO mice, compared to WT animals at 3 weeks of age. Data were normalized to Gapdh. Data represent means ± SEM from four WT, eight *Pum1*-Het, and four *Pum1*-KO mouse brains, with equal numbers of males and females for each genotype.

(E) qPCR of *SNCA*, *PUM1*, and *FEV* (negative control) after knockdown or overexpression (OE) of *PUM2* in HEK293T cells. Data were normalized to *GAPDH* and then compared to cells treated with an empty vector for *PUM2* overexpression and siScramble for *PUM2* knockdown experiments.

Statistical significance was determined by ANOVA and Student's t test: $^{*}p < 0.05$, $^{**}p < 0.01$, $^{***}p < 0.001$.

redistribution of *Snca*: *Snca* mRNA fell by ~25% in the soma but rose almost 50% in the axon (Figure 4C). These data indicate that Pum1 regulation of *Snca* is conserved in rat neurons and that Pum1 safeguards the axons against α-Syn accumulation.

PUM1 represses α-Syn expression in neurons derived from patients with *SNCA* triplication

We reprogrammed human induced pluripotent stem cells (hiSPCs) from patients carrying triplications of the *SNCA* locus into induced neurons (iNs) (see STAR Methods). These patients

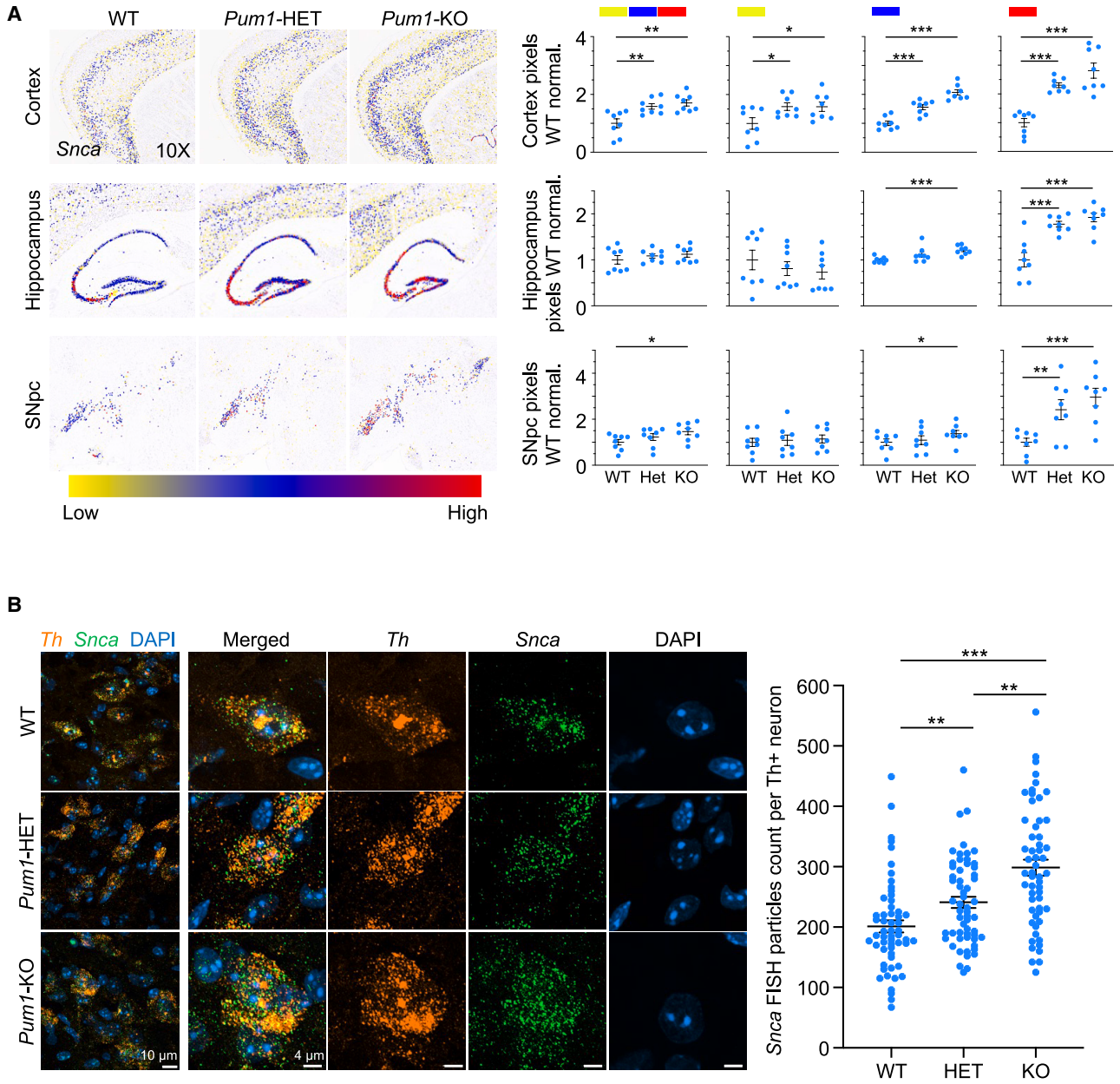

Figure 3. *Pum1* haploinsufficiency increases *Snca* RNA levels in specific brain regions and in individual neurons within the SNpc

(A) Magnified representative ISH sagittal images of *Snca* in the cortex, hippocampus, and substantia nigra pars compacta from WT, *Pum1*-Het, and *Pum1*-KO mouse cortex, hippocampus, and substantia nigra pars compacta (SNpc), taken from whole-brain images (Figure S3). The intensity of the ISH signal is color coded on a yellow-to-red gradient (low, yellow; medium, blue; high, red). Graphs to the right: the first column shows the total number of painted pixels; columns 2 through 4 show low-intensity (yellow), medium-intensity (blue), and high-intensity (red) bins, indicated by the color bar at the top of each panel (see STAR Methods). Each dot represents a single quantified section, with a total of eight sections per genotype. See also Figures S2, S4, and S5.

(B) Representative RNAscope FISH images of coronal brain sections at 40× objective highlighting individual dopaminergic neurons from WT, *Pum1*-Het, and *Pum1*-KO mice at 3 weeks of age. A single *Th*-positive neuron is selected from the left panel (scale bar, 10 μm) of each genotype and shown in individual channels (merged, *Th*, *Snca*, and DAPI) in the right panels (scale bar, 4 μm). Each fluorescent particle on *Snca* channel represents one *Snca* mRNA molecule. Quantification of *Snca* mRNA particles per Th^+ neuron for each genotype is shown on the right. Only non-overlapping, fully imaged Th^+ neurons were included in the analysis. Each dot represents a single Th^+ neuron: WT ($n = 56$ neurons), *Pum1*-Het ($n = 58$ neurons), and *Pum1*-KO ($n = 56$ neurons), with three mice per genotype. See also Figure S3.

Data represent means ± SEM. Statistical significance was determined by ANOVA and Student's t test: $^*p < 0.05$, $^{**}p < 0.01$, $^{***}p < 0.001$. See also Figures S2–S4.

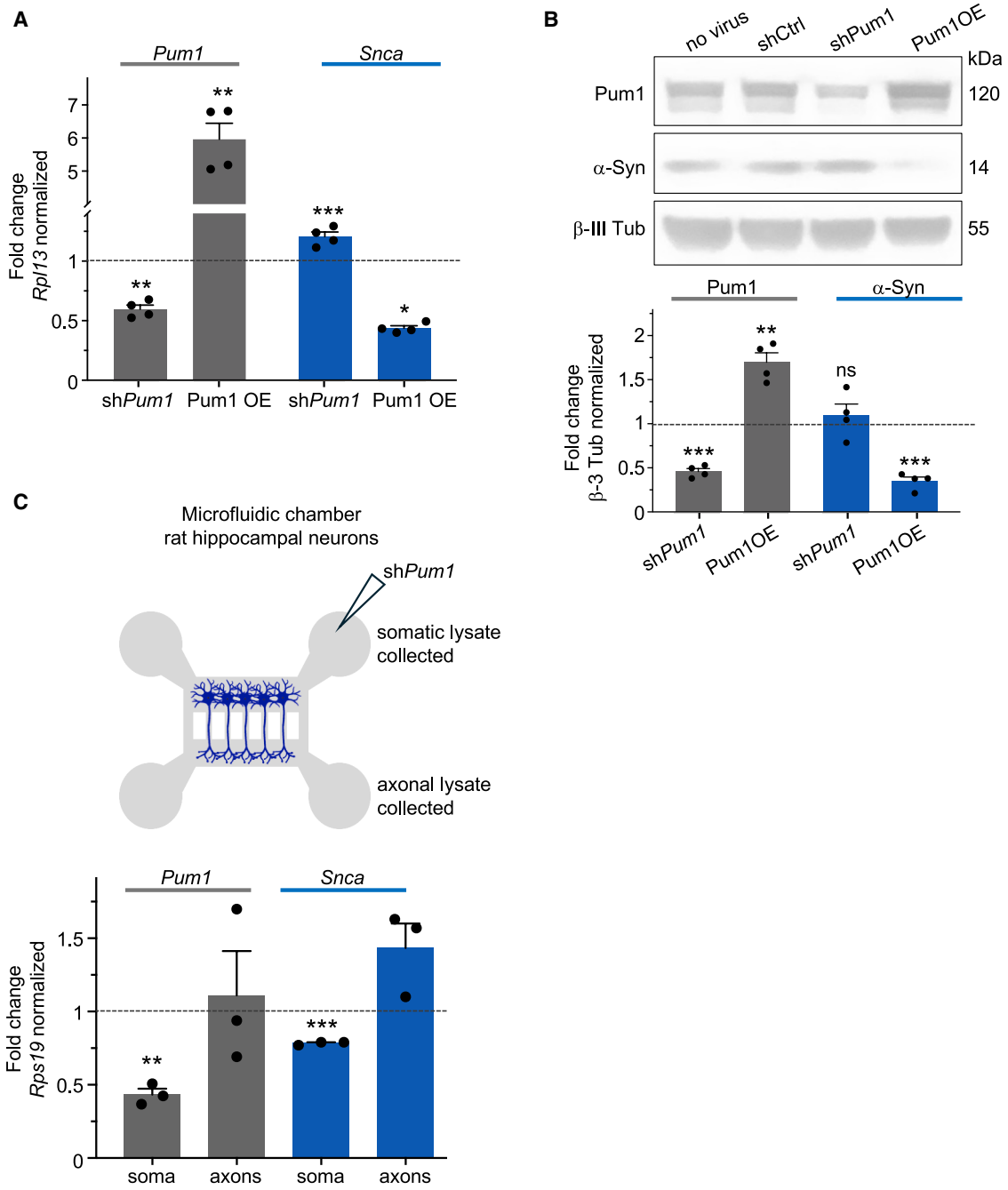

Figure 4. *Pum1* regulates α-Syn levels in rat hippocampal neurons

(A and B) sh*Pum1* and Pum1 were virally delivered to primary rat hippocampal neurons and compared to a non-targeting control shRNA or empty vector, respectively (dotted line). (A) *Snca* and *Pum1* mRNA and (B) α-Syn protein levels were then quantified as described in STAR Methods. *Snca* mRNA and α-Syn protein levels were reduced following Pum1 overexpression (OE) compared to the empty vector. Conversely, neurons transduced with sh*Pum1* showed a modest upregulation of both *Snca* mRNA and α-Syn protein. Data represent means ± SEM from three biological replicates. Statistical significance was determined by Student's t test: $^{*}p < 0.05$, $^{**}p < 0.01$, $^{***}p < 0.001$.

(C) Top: schematic representation of the microfluidic chamber. Primary rat hippocampal neurons were cultured in the upper compartment and extended axons through 750-μm-long microgrooves into the axonal compartment. We administered sh*Pum1* or shControl lentiviruses into the somatic compartment to knock down *Pum1* before cell lysis and RNA quantification. Bottom: qPCR shows that *Pum1* mRNA was reduced >50% in the soma but unaffected in the axons compared to shControl. *Snca* levels fell in the soma but were increased in the axons. Data were normalized to *Rps19* mRNA levels. One-sample t test on fold-change values in each column compared to a hypothetical value of 1 (dotted line representing shControl); $^{**}p < 0.01$, $^{***}p < 0.001$.

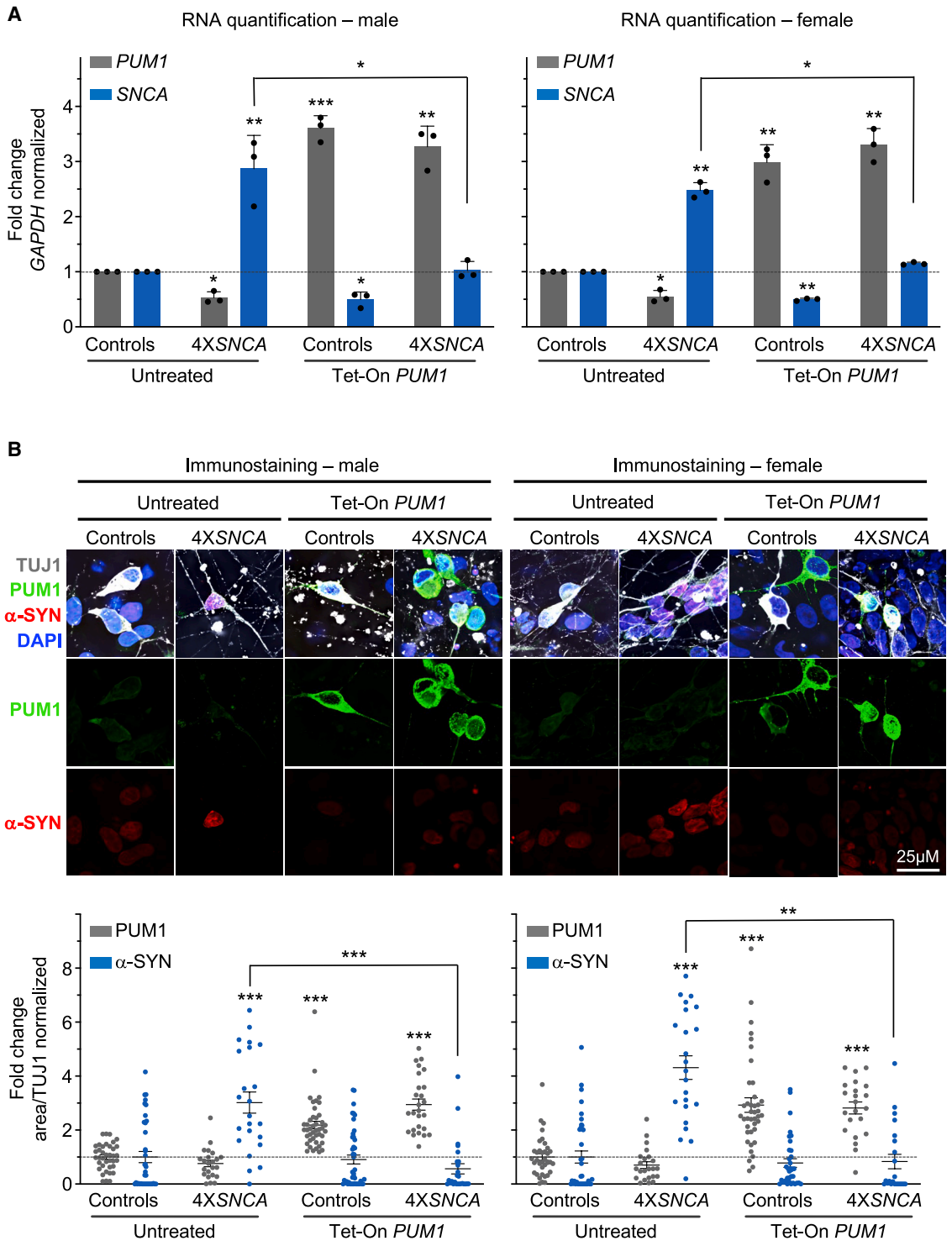

Figure 5. PUM1 regulates α-Syn in human PD neurons

(A) Quantification of *PUM1* and *SNCA* mRNA by qPCR in male (left) and female (right) reprogrammed PD neurons and their respective isogenic controls, with and without *PUM1* transfection. Data were normalized to *GAPDH* and compared to untreated control neurons.

(B) Immunostaining (upper panels) and relative signal quantification (lower graphs) in male (left) and female (right) neurons reprogrammed from controls and patients with PD with *SNCA* triplication (four alleles, or 4× *SNCA*) and their isogenic controls. Staining for TUJ1 (purple), encoded by *TUBB3*, was used as a

(legend continued on next page)

have a genetic form of PD, as they carry a triplication of the *SNCA* locus (leading to four copies of the gene instead of two).[30] For each patient we generated isogenic control cell lines using CRISPR-Cas9 to create hiPSC lines with two copies of *SNCA*.[30,31] These lines stably integrated the Tet-On doxycycline-inducible transcription factor NGN2 (Tet-On NGN2), enabling rapid transdifferentiation into iNs.[30,31] The hiPSC lines were reprogrammed into iNs, followed by transduction of Tet-On *PUM1* at 14 days *in vitro* (DIV 14) and were maintained with a low amount of doxycycline until DIV 21. These were compared to untreated control lines (see STAR Methods and Figure S5A). Neuronal reprogramming was confirmed by staining for MAP2 and TUBB3[32–34] (Figure S5B).

In the untreated condition, *SNCA* mRNA levels were three times higher in PD neurons than in their sex-matched controls, while *PUM1* mRNA levels in these PD neurons were 50% lower (Figure 5A). Treating with doxycycline (Tet-On *PUM1*) reduced *SNCA* mRNA in controls by roughly 50% but normalized *SNCA* mRNA levels in both male and female patient iNs (Figure 5A). We then quantified immunofluorescence intensity to gauge α-Syn levels. Untreated PD iNs overall had elevated α-Syn levels, but transduction with PUM1 reduced α-Syn levels to those observed in sex-matched controls (Figure 5B). We were intrigued by the fact that in healthy controls, the doxycycline treatment did not reduce protein levels (and reduced mRNA by only 50%, whereas in PD iNs mRNA was reduced 60%–67%). We hypothesized that the explanation could involve a change in how much of the pool of *SNCA* mRNA consists of the long 3′ UTR isoform. The long isoform, having two PREs, will be most responsive to changes in PUM1 concentrations, while shorter isoforms with only one PRE will have a modest response, and those lacking PREs entirely will not be affected by PUM1 at all. If the PD cells have proportionally more of the long *SNCA* isoform, they will be more susceptible to regulation by PUM1.

In healthy controls, the ratio of *SNCA* with a long 3′ UTR to the total *SNCA* mRNA is just under 1:1, but in sporadic PD the ratio favors the long isoform.[14] We were curious as to whether the same is true in the case of *SNCA* locus triplication, so we assessed the relative abundance of these isoforms in our PD iNs using primers that either bind to a distal sequence, bind to capture the long isoform (“long *SNCA*”), or bind to a sequence just beyond the last exon, which will capture all but the very shortest *SNCA* mRNA (“total *SNCA*”) (Figure S5C; see STAR Methods). In PD iNs from both males and females, all mRNA isoforms were upregulated, with long *SNCA* showing a greater increase after normalization to *GAPDH* than the total *SNCA* (Figure S5C); doxycycline treatment (Tet-On *PUM1*) reduced *SNCA* mRNA overall but exerted a greater effect on the long isoform, which contains two PREs rather than one (Figure 1E; quantification provided in the legend). PUM1 does not alter the choice of polyadenylation site, i.e., how much of the long isoform is generated relative to the total *SNCA* mRNA (Figure S5D). These data confirm that the long isoform is somehow favored in PD—to an even greater extent in genetic PD than in sporadic disease[14]—but that augmenting PUM1 can restore normal *SNCA* and α-Syn levels.

PUM1 and *SNCA* mRNA levels anti-correlate in specific cell types within the human SNpc

The loss of dopaminergic neurons in the SNpc is a defining pathological feature of both genetic and sporadic forms of PD. To investigate the relationship between *SNCA* and *PUM1* expression in the human SNpc, we analyzed a recent single-nucleus RNA sequencing (snRNA-seq) dataset of dopaminergic neurons obtained from postmortem patients and healthy controls.[35] To address the technical challenges of dropout events and zero inflation in snRNA-seq data, we employed a meta-cell approach,[36] which groups closely related cells into composite entities by averaging their raw count matrices. This was followed by permutation testing to establish an empirical null distribution for the correlation of expression levels between genes of interest (see STAR Methods).

Our analysis revealed a significant inverse correlation between *PUM1* and *SNCA* expression (Figures 6A and S6A). *SNCA* showed no such relationship with the pan-dopaminergic marker control *SLC18A2*, which encodes the vesicular transporter VMAT2 (Figure 6B and S6B). We found a weaker but still significant anti-correlation between *PUM2* and *SNCA* (rho = −0.093 vs. −0.265 for *PUM1*) (Figures 6C and S6C). The combined correlation (*PUM1* + *PUM2*, rho = −0.236) confirms the dominant effect of PUM1 in this inverse relationship with *SNCA* in SNpc neurons (Figures 6D and S6D).

Given that the SNpc contains several subpopulations of dopaminergic cells,[35] each expressing different markers, we analyzed the expression pattern of *PUM1*, *PUM2*, and *SNCA* by cell type. *PUM1* and *SNCA* expression appeared inversely correlated in most cell types, while *PUM2* and *SLC18A2* (used here as control) largely did not (Figure 6E). The *SOX6_AGTR1* cluster, which suffers the greatest loss of cells in patients with PD or Lewy body dementia,[35] had both the lowest levels of *PUM1* and the highest levels of *SNCA* as well as *AGTR1*, as would be expected (Figure 6F). In contrast, *PUM1* was upregulated and *SNCA* downregulated in the *CALB1_TRHR* subtype, which is enriched in the dorsal tier of the SNpc and is less vulnerable in PD[35] (Figure 6E).

SNCA repression by miR-7 requires PUM1

PUM1 interacts with the miRNA machinery through AGO2, which plays a key catalytic role in mRNA degradation as part of the RNA-induced silencing complex (RISC).[27] To investigate whether AGO2 and miRNAs play a role in PUM1-driven *SNCA* repression, we treated WT HEK293T cells with small interfering RNA (siRNA) against *PUM1* or overexpressed *PUM1*, followed by siRNA against *AGO2* (Figures S7A–S7D). As expected, *PUM1* overexpression decreased α-Syn levels, while *AGO2*

neuron-specific marker for internal quantification. DAPI staining (blue) was used as an internal control to label the nuclei, while staining for PUM1 (green) and α-Syn (red) was used to quantify their levels in PD reprogrammed neurons compared to their respective isogenic healthy controls with two *SNCA* alleles. Data represent the mean ± SEM from three technical and biological replicates (indicated here as single dots). Statistical significance was calculated using Student’s t test: $^{*}p < 0.05$, $^{**}p < 0.01$, $^{***}p < 0.001$. See also Figure S5.

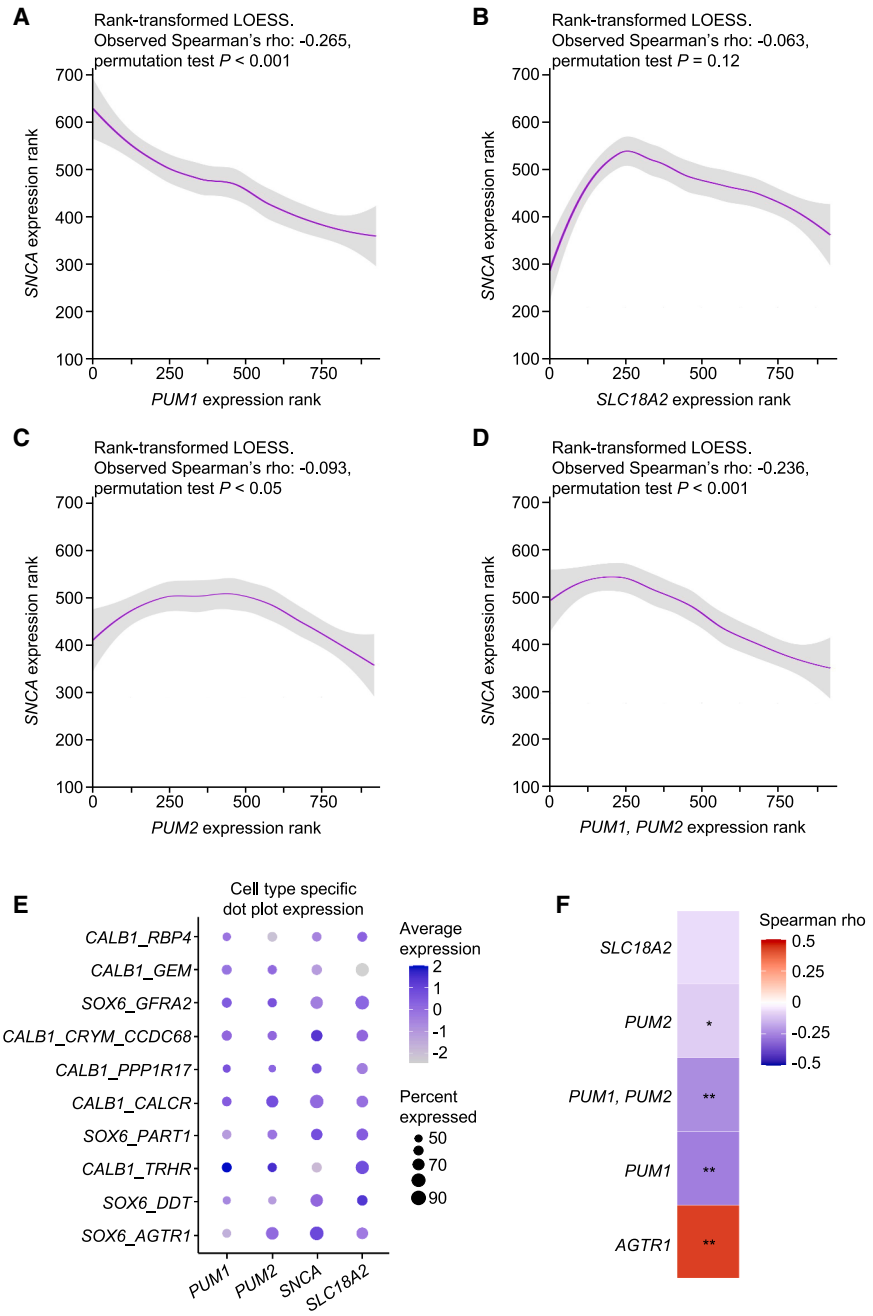

Figure 6. *PUM1* and *SNCA* are anti-correlated in human dopaminergic neurons in the substantia nigra pars compacta

(A–D) Locally estimated scatterplot smoothing (LOESS) plot of (A) *PUM1* against *SNCA*, (B) *SLC18A2* (used here as comparator) against *SNCA*, (C) *PUM2* against *SNCA*, and (D) *PUM1* + *PUM2* against *SNCA* from single-nucleus RNA-seq of human samples shows a significant anti-correlation.

(E) Dotplot showing *PUM1*, *PUM2*, *SNCA*, and *SLC18A2* mRNA.

(F) Summary of the Spearman rho correlation of *PUM1*, *PUM2*, *SLC18A2*, and *AGTR1*, against *SNCA* mRNA in the SNpc (used here as positive control). Statistical significance was calculated using a permutation test: $^{*}p < 0.05$, and $^{**}p < 0.01$. See also Figure S6.

silencing increased them (Figure S7A). *PUM1* overexpression with silenced *AGO2* restored α-Syn levels to WT (Figure S7A). Furthermore, silencing both *PUM1* and *AGO2* led to a greater fold-change increase in α-Syn than the loss of either alone (Figure S7B). The same effect was observed at the mRNA level (Figures S7C and S7D), suggesting that PUM1 and AGO2 co-regulate *SNCA* mRNA.

Among the several miRNAs that have been predicted to regulate *SNCA*, only miR-7 has been shown to play a role in PD,[7,9–11] although the precise mechanisms are unclear. We therefore tested whether miR-7 regulation could be influenced by the presence of PUM1. Overexpression of miR-7 or *PUM1* alone in WT HEK293T cells reduced *SNCA* mRNA and α-Syn protein levels (Figures 7A and S7E). The combined overexpression of miR-7 and *PUM1* led to a greater reduction in α-Syn than either PUM1 or miR-7 alone (Figures 7A and S7E). Interestingly, miR-7 overexpression was able to limit the degree of α-Syn increase caused by *PUM1* knockdown (Figures 7B and S7F). To determine whether PUM1 and miR-7 function independently or in concert, we quantified *SNCA* mRNA levels in *PUM1*-KO HCT116 cells following miR-7 overexpression. Strikingly, miR-7 overexpression was unable to reduce *SNCA* mRNA levels in *PUM1*-KO cells, but it did so in WT cells (Figure 7C). These data indicate that miR-7 requires PUM1 to regulate *SNCA*.

PD databases contain subjects bearing *PUM1* variants

The above results suggest that variants in the 3′ UTR that disturb one or both PREs might contribute to some cases of sporadic PD by preventing PUM1 from regulating *SNCA*. Unfortunately, because the exome and genome dataset we were able to work with was delimited for coding regions only, we were not able to assess the 3′ UTR. As a proxy, then, to find out whether loss of PUM1 regulation might contribute to PD, we searched clinical databases for PUM1 variants (see STAR Methods). We extracted *PUM1* coding variants from 3,484 exomes or genomes of patients with PD and filtered for variants that are absent or very rare in control databases (Table S3). There were 26 subjects bearing 25 different PUM1 variants, and of these, five variants did not appear at all in the non-PD controls (Table S3). Given that PD is a late-onset disease, it remains possible that some of the healthy control

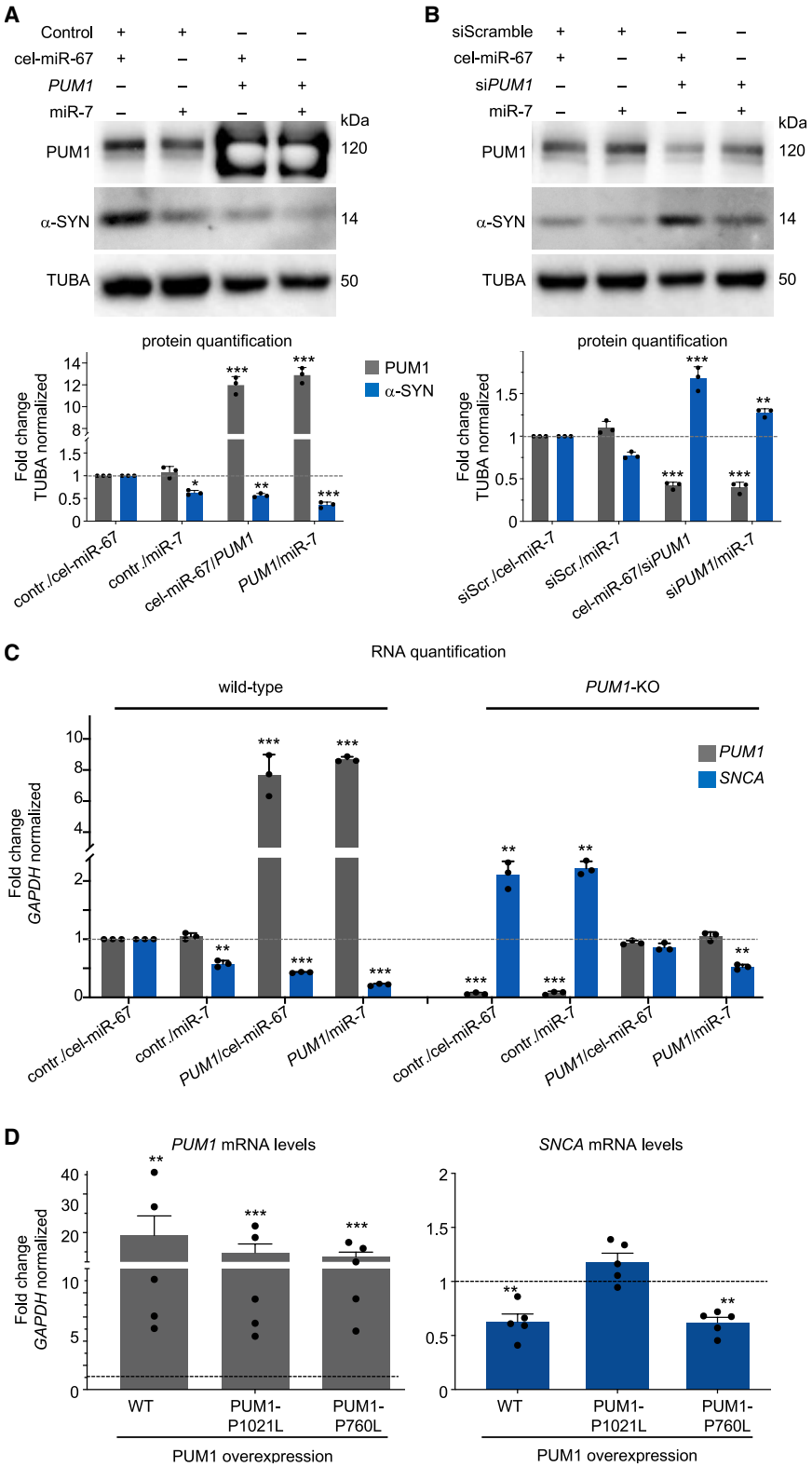

Figure 7. miR-7 requires PUM1 to regulate α-Syn

(A and B) Representative western blot and relative quantification of PUM1 and α-Syn in HEK293T cells following either *PUM1* or miR-7 overexpression alone or together (A), or after *PUM1* knockdown (si*PUM1*) or miR-7 overexpression alone or together (B). Data were normalized to tubulin (TUBA) protein levels and represent means ± SEM from three biological replicates. Empty vector (control) and siScramble were used for overexpression and knockdown experiments, respectively. Cel-miR-67 was used as a negative control for miR-7 overexpression.

(C) qPCR of *PUM1* and *SNCA* following either *PUM1* or miR-7 overexpression alone or together in WT or *PUM1*-KO HCT116 cell lines. *SNCA* is elevated in *PUM1*-KO cell lines, with re-introduction of PUM1 reducing levels to WT. miR-7 overexpression does not decrease *SNCA* mRNA in the absence of *PUM1*. Data were normalized to *GAPDH* and represent means ± SEM from three biological replicates.

(D) RNA quantification of *PUM1* and *SNCA* after transfection with 200–400 ng of either *PUM1*-WT, *PUM1*-P760L, and *PUM1*-P1021L in HEK293T cells. Data were normalized to *GAPDH* and non-transfected cell lines and represent means ± SEM from three biological replicates. Statistical significance was determined using Student's t test: $^{*}p < 0.05$, $^{**}p < 0.01$, $^{***}p < 0.001$. See also Figure S7.

patients will develop a neurodegenerative condition in the future (either PD or the late-onset ataxia caused by certain PUM1 variants).

We selected two of the 25 variants, one that was unique to the PD cohort (p.P1021L) and another that was also found in two subjects in gnomAD (p.P760L), and cloned and tested them in HEK293T cells. Both WT PUM1 and variant p.P760L, which affects a disordered region of the protein, reduced *SNCA* mRNA, but p.P1021L, which alters PUM1's RNA-binding domain, was unable to suppress *SNCA* mRNA (Figures 7D and 7E). It is therefore possible that variation in PUM1 or in the *SNCA* 3′ UTR that alters PUM1 target binding contributes to some cases of sporadic PD.

DISCUSSION

The heritability of PD has been considered relatively low (~15%) compared to that of other neurodegenerative diseases (e.g., Alzheimer's may be 58%–79% heritable),[37] despite over 20 genes having been associated with monogenic forms of PD and there being over 90 risk loci. The current study, however, adds to a growing body of literature[12,38–40] indicating that variants in the 3′ UTR of *SNCA* contribute to the development of PD. Unfortunately, the genome analyses most frequently used in patients (exome sequencing and copy-number variation) overlook non-coding regions of genes.

There remains much to be understood about α-Syn regulation, which is enormously complex, and its differential accumulation in various synucleinopathies. For example, it remains unclear why α-Syn accumulates in dopaminergic neurons in the substantia nigra in PD but in oligodendrocytes in MSA and in cortical or hippocampal tissues in Lewy body dementia.[41,42] In this study, certain neuronal subtypes within the mouse SNpc exhibited varying degrees of inverse correlation between *PUM1* and *SNCA*. This indicates that PUM1 regulation of *SNCA* is influenced by cell-specific factors that have yet to be discovered. Our data showing that PUM2 is not expressed in the SNpc indicate that part of the answer is differential expression of RBPs and other regulatory factors in different regions or cell types. These results also point to the critical importance of examining regulatory relationships *in vivo*.

Interestingly, our microfluidic chamber experiments with cultured rat neurons suggested that Pum1 influences the compartment-specific localization of *Snca* mRNA in a manner reminiscent of its homolog Pum2.[29] This spatial regulation is particularly significant in neurons, which are exquisitely sensitive to changes in compartment-specific gene expression—a factor increasingly linked to neurodegenerative processes.[43] Moreover, since RNA stability can be affected by subcellular localization,[44] Pum1-mediated positioning of *Snca* mRNA could further influence its regulation and accumulation. For example, iPSC-derived midbrain dopaminergic neurons taken from patients bearing *SNCA* duplications show greater translocation of *SNCA* from the soma to neurites, along with compromised neurite integrity.[45,46] Too much axonal *SNCA* translation could trigger aggregation or exocytic propagation.

Our data suggest that future studies should focus on region- and cell-specific differences in the 3′ UTR of *SNCA* and other PD-associated genes, where mutations in RBP or miRNA regulatory elements would remove an important mechanism for regulating α-Syn. In this context, it is worth noting that a study on cerebral amyloid angiopathy found that a 2-nt deletion in the 3′ UTR of *APP*, one of the genes we found to be regulated by PUM1, leads to overexpression of amyloid precursor protein[47]—and we notice that this deletion alters a PRE. Whether loss of PUM1 regulation is the sole or main cause of APP accumulation in these patients warrants further study. The fact that at least some individuals with PD carry *PUM1* variants supports the notion that disruptions in the post-transcriptional regulation of *SNCA* and other PD-related genes could help explain at least a portion of PD cases that currently appear idiopathic.

Consideration should also be given to additional endogenous and exogenous factors that have been associated with altered risk of PD. For example, Rhinn et al. found that dopamine increases the usage of the *SNCA* long 3′ UTR, which is associated with α-Syn accumulation and PD pathology.[14] The same study showed that environmental risk factors for PD, such as rotenone, similarly increase the proportion of longer *SNCA* 3′ UTR isoforms, whereas protective exposures like nicotine reduce it.[14] Our current finding that the long isoform forms a greater proportion of the total *SNCA* mRNA pool in iNs from patients with PD compared to healthy controls, which underscores the importance of understanding what determines this rise in the longer isoform and why it is problematic. Furthermore, given that we and others observed that upregulation of α-Syn co-occurs with downregulation of miR-7[9,11] and PUM1 (the current study), it is worth asking whether there could be bidirectional influence between α-Syn and its repressors. It may be, for instance, that α-Syn upregulation begins as a compensatory response that then leads to downstream pathology. Much further study is needed but, altogether, these provocative results emphasize the necessity of unraveling the complex regulatory mechanisms that govern α-Syn expression *in vivo* in specific contexts.

Limitations of the study

Our study does not attempt to find other RBPs that regulate *SNCA*, either in coordination with or independently of PUM1. Similarly, other miRNAs, including those previously implicated in *SNCA* mRNA regulation and binding,[7,48] likely coordinate with PUM1 or other RNA-binding proteins. While we have identified PD cases involving *de novo* mutations in the RNA-binding domain of *PUM1*, analysis of the *SNCA* 3′ UTR sequence and length in patients with PD remains limited.

RESOURCE AVAILABILITY

Lead contact

Requests for further information and resources should be directed to and will be fulfilled by the lead contact, Vincenzo A. Gennarino (vag2138@cumc.columbia.edu).

Materials availability

All unique/stable reagents generated in this study are available from the lead contact without restriction. No unique reagents were generated as part of this study. The mouse lines used in this study have already been published[15,16] and are available upon approval of a material transfer agreement.

Data and code availability

- All source data and quantifications related to this article are available at Mendeley: https://data.mendeley.com/datasets/4km8t9w7jy/1.
- Any additional information required to reanalyze the data reported in this paper is available from the lead contact upon request.

ACKNOWLEDGMENTS

This work began in the lab of Huda Y. Zoghbi, whom we thank for her support. We also thank Cecilia Ljungberg for ISH analysis and members of the Gennarino laboratory for helpful discussions. We thank Roy Alcaly, Karen Marder, and the staff of the Columbia Movement Disorder Division as well as the Institute of Genomic Medicine for access to the PD exome sequencing data, supported by the National Institute of Neurological Disorders and Stroke (NINDS; NS032527 and NS036630), the Parkinson's Foundation, and the Michael J. Fox Foundation. The current work was supported by NINDS (R01NS109858 to V.A.G.); the National Institute of General Medical Sciences (NIGMS; T32GM007088 to M.C.); the National Center for Advancing Translational Sciences (NCATS; TL1TR001875 to M.C.); NINDS (F31NS113574 to L.K.R.); NINDS (T32NS064928 to L.K.R.); NINDS (R01NS125018 to C.Z.); NIGMS (R35GM145279 to C.Z.); the National Institute of Mental Health (NIMH; 1T32NS115699 to L.K.R., PI: W.B.G.); NINDS (R01NS128142 to V.K.); NINDS (R01NS119690 to R.A.); the National Institute on Aging (NIA; T32AG000222-23 to X.W.); the National Cancer Institute (NCI; R01CA251753-01 to W.M); a National Ataxia Foundation/Young Investigator Research grant (V.A.G.); a TIGER award, the Taub Institute, and Columbia University Irving Medical Center (V.A.G. and U.H.); Paul A. Marks Scholar Program and Columbia University Vagelos College of Physicians and Surgeons (V.A.G.); Neurodegeneration Challenge Network/Chan Zuckerberg Initiative (CZI) (V.A.G.); a Taub Institute grant for emerging research (U.H.); and the American Cancer Society (ACS; RSG-20-060-01-RMC to W.M.). This project was also supported by the RNA In Situ Hybridization Core at Baylor College of Medicine, which is, in part, supported by a Shared Instrumentation grant from the NIH Tecan EVO GenePaint robot (S10OD016167).

Data used in this article were acquired from internal Parkinson's disease clinical databases at Columbia University Irving Medical Center. We thank Richard P. Mayeux, MD; Karen S. Marder, MD, MPH; Roy N. Alcalay, MD; and Helen Mejia-Santana for access to these databases. Additional data were obtained from the Accelerating Medicine Partnership (AMP); please see supplemental acknowledgments (Methods S1).

AUTHOR CONTRIBUTIONS

M.C.: formal analysis, validation, visualization, methodology, and writing – original draft. P.G.M.: formal analysis, validation, visualization, and writing – review & editing. Z.A.G.: formal analysis, methodology, and writing – review & editing. R.W.: formal analysis, validation, and visualization. M.M.P.: formal analysis, validation, and visualization. L.K.R.: formal analysis and writing – review & editing. C.G.R.: formal analysis and writing – review & editing. S.F.: formal analysis, data curation, and writing – review & editing. S.R.: formal analysis, validation, and visualization. N.d.P.: formal analysis, validation, visualization, and writing – review & editing. A.C.: methodology and writing – review & editing. X.W.: resources and writing – review & editing. R.K.S.: formal analysis, validation, investigation, and writing – review & editing. S.R.: formal analysis, validation, and writing – review & editing. H.K.Y.: formal analysis, data curation, and writing – review & editing. W.M.: formal analysis, data curation, and writing – review & editing. K.B.: resources and writing – review & editing. C.Z.: formal analysis, data curation, and visualization. M.B.H.: data curation and formal analysis. V.K.: resources, data curation, and writing – review & editing. V.B.: conceptualization, analysis, visualization, and writing – review & editing. U.H.: formal analysis, data curation, visualization, and writing – review & editing. R.A.: resources, data curation, and writing – review & editing. V.A.G.: conceptualization, resources, data curation, formal analysis, supervision, funding acquisition, validation, investigation, visualization, methodology, writing – original draft, project administration, and writing – review & editing.

DECLARATION OF INTERESTS

V.K. is a co-founder of DaCapo Brainscience, a company involved in neurodegenerative disease research.

STAR★METHODS

Detailed methods are provided in the online version of this paper and include the following:

- KEY RESOURCES TABLE
- EXPERIMENTAL MODEL AND STUDY PARTICIPANT DETAILS
  - RNA-cross linking immunoprecipitation (CLIP)
  - *In situ* hybridization and analysis
  - RNAscope
  - Lentivirus preparation and neuronal transduction
  - Single nuclei RNA sequencing from patients
  - Search of clinical databases for individuals with PD carrying *PUM1* variants
  - Animals
- METHOD DETAILS
  - Cell culture
  - Cell transfection
  - Immunocytochemical assays
  - RNA extraction and quantitative real-time PCR
  - Protein extraction and western blot
  - Luciferase assay
  - Microfluidic chamber assay
- QUANTIFICATION AND STATISTICAL ANALYSIS
  - Experimental design
  - Statistical analysis

SUPPLEMENTAL INFORMATION

Supplemental information can be found online at https://doi.org/10.1016/j.celrep.2025.116145.

Received: January 24, 2025
Revised: June 9, 2025
Accepted: July 23, 2025
Published: August 13, 2025

REFERENCES

1. Hickman, R.A., Faust, P.L., Marder, K., Yamamoto, A., and Vonsattel, J.P. (2022). The distribution and density of Huntingtin inclusions across the Huntington disease neocortex: regional correlations with Huntingtin repeat expansion independent of pathologic grade. Acta Neuropathol. Commun. *10*, 55. https://doi.org/10.1186/s40478-022-01364-1.
2. Ibanez, P., Lesage, S., Janin, S., Lohmann, E., Durif, F., Destee, A., Bonnet, A.M., Brefel-Courbon, C., Heath, S., Zelenika, D., et al. (2009). Alpha-synuclein gene rearrangements in dominantly inherited parkinsonism: frequency, phenotype, and mechanisms. Arch. Neurol. *66*, 102–108. https://doi.org/10.1001/archneurol.2008.555.
3. Caramiello, A.M., and Pirota, V. (2024). Novel Therapeutic Horizons: SNCA Targeting in Parkinson's Disease. Biomolecules *14*, 949. https://doi.org/10.3390/biom14080949.
4. Galvin, J.E., Lee, V.M., and Trojanowski, J.Q. (2001). Synucleinopathies: clinical and pathological implications. Arch. Neurol. *58*, 186–190. https://doi.org/10.1001/archneur.58.2.186.
5. McCann, H., Stevens, C.H., Cartwright, H., and Halliday, G.M. (2014). alpha-Synucleinopathy phenotypes. Parkinsonism Relat. Disord. *20*, S62–S67. https://doi.org/10.1016/S1353-8020(13)70017-8.
6. Guhathakurta, S., Bok, E., Evangelista, B.A., and Kim, Y.S. (2017). Deregulation of alpha-synuclein in Parkinson's disease: Insight from epigenetic

structure and transcriptional regulation of SNCA. Prog. Neurobiol. *154*, 21–36. https://doi.org/10.1016/j.pneurobio.2017.04.004.

7. Mouradian, M.M. (2012). MicroRNAs in Parkinson's disease. Neurobiol. Dis. *46*, 279–284. https://doi.org/10.1016/j.nbd.2011.12.046.
8. Snoderly-Foster, L.J., and Olivas, W.M. (2022). Regulation of Parkinson's disease-associated genes by Pumilio proteins and microRNAs in SH-SY5Y neuronal cells. PLoS One *17*, e0275235. https://doi.org/10.1371/journal.pone.0275235.
9. Junn, E., Lee, K.W., Jeong, B.S., Chan, T.W., Im, J.Y., and Mouradian, M.M. (2009). Repression of alpha-synuclein expression and toxicity by microRNA-7. Proc. Natl. Acad. Sci. USA *106*, 13052–13057. https://doi.org/10.1073/pnas.0906277106.
10. Choi, D.C., Yoo, M., Kabaria, S., and Junn, E. (2018). MicroRNA-7 facilitates the degradation of alpha-synuclein and its aggregates by promoting autophagy. Neurosci. Lett. *678*, 118–123. https://doi.org/10.1016/j.neulet.2018.05.009.
11. McMillan, K.J., Murray, T.K., Bengoa-Vergniory, N., Cordero-Llana, O., Cooper, J., Buckley, A., Wade-Martins, R., Uney, J.B., O'Neill, M.J., Wong, L.F., and Caldwell, M.A. (2017). Loss of MicroRNA-7 Regulation Leads to alpha-Synuclein Accumulation and Dopaminergic Neuronal Loss In Vivo. Mol. Ther. *25*, 2404–2414. https://doi.org/10.1016/j.ymthe.2017.08.017.
12. Marchese, D., Botta-Orfila, T., Cirillo, D., Rodriguez, J.A., Livi, C.M., Fernández-Santiago, R., Ezquerra, M., Martí, M.J., Bechara, E., and Tartaglia, G.G.; Catalan MSA Registry CMSAR (2017). Discovering the 3′ UTR-mediated regulation of alpha-synuclein. Nucleic Acids Res. *45*, 12888–12903. https://doi.org/10.1093/nar/gkx1048.
13. Kattan, F.G., Koukouraki, P., Anagnostopoulos, A.K., Tsangaris, G.T., and Doxakis, E. (2023). RNA binding protein AUF1/HNRNPD regulates nuclear export, stability and translation of SNCA transcripts. Open Biol. *13*, 230158. https://doi.org/10.1098/rsob.230158.
14. Rhinn, H., Qiang, L., Yamashita, T., Rhee, D., Zolin, A., Vanti, W., and Abeliovich, A. (2012). Alternative alpha-synuclein transcript usage as a convergent mechanism in Parkinson's disease pathology. Nat. Commun. *3*, 1084. https://doi.org/10.1038/ncomms2032.
15. Gennarino, V.A., Singh, R.K., White, J.J., De Maio, A., Han, K., Kim, J.Y., Jafar-Nejad, P., di Ronza, A., Kang, H., Sayegh, L.S., et al. (2015). Pumilio1 haploinsufficiency leads to SCA1-like neurodegeneration by increasing wild-type Ataxin1 levels. Cell *160*, 1087–1098. https://doi.org/10.1016/j.cell.2015.02.012.
16. Gennarino, V.A., Palmer, E.E., McDonell, L.M., Wang, L., Adamski, C.J., Koire, A., See, L., Chen, C.A., Schaaf, C.P., Rosenfeld, J.A., et al. (2018). A mild PUM1 mutation is associated with adult-onset ataxia, whereas haploinsufficiency causes developmental delay and seizures. Cell *172*, 924–936.e11. https://doi.org/10.1016/j.cell.2018.02.006.
17. Goldstrohm, A.C., Hall, T.M.T., and McKenney, K.M. (2018). Post-transcriptional Regulatory Functions of Mammalian Pumilio Proteins. Trends Genet. *34*, 972–990. https://doi.org/10.1016/j.tig.2018.09.006.
18. Galgano, A., Forrer, M., Jaskiewicz, L., Kanitz, A., Zavolan, M., and Gerber, A.P. (2008). Comparative analysis of mRNA targets for human PUF-family proteins suggests extensive interaction with the miRNA regulatory system. PLoS One *3*, e3164. https://doi.org/10.1371/journal.pone.0003164.
19. Enwerem, I.I.I., Elrod, N.D., Chang, C.T., Lin, A., Ji, P., Bohn, J.A., Levdansky, Y., Wagner, E.J., Valkov, E., and Goldstrohm, A.C. (2021). Human Pumilio proteins directly bind the CCR4-NOT deadenylase complex to regulate the transcriptome. RNA *27*, 445–464. https://doi.org/10.1261/rna.078436.120.
20. Van Etten, J., Schagat, T.L., Hrit, J., Weidmann, C.A., Brumbaugh, J., Coon, J.J., and Goldstrohm, A.C. (2012). Human Pumilio proteins recruit multiple deadenylases to efficiently repress messenger RNAs. J. Biol. Chem. *287*, 36370–36383. https://doi.org/10.1074/jbc.M112.373522.
21. Kramer, A., Green, J., Pollard, J., Jr., and Tugendreich, S. (2014). Causal analysis approaches in Ingenuity Pathway Analysis. Bioinformatics *30*, 523–530. https://doi.org/10.1093/bioinformatics/btt703.
22. Maraganore, D.M., Lesnick, T.G., Elbaz, A., Chartier-Harlin, M.C., Gasser, T., Krüger, R., Hattori, N., Mellick, G.D., Quattrone, A., Satoh, J.I., et al. (2004). UCHL1 is a Parkinson's disease susceptibility gene. Ann. Neurol. *55*, 512–521. https://doi.org/10.1002/ana.20017.
23. Clausen, L., Okarmus, J., Voutsinos, V., Meyer, M., Lindorff-Larsen, K., and Hartmann-Petersen, R. (2024). PRKN-linked familial Parkinson's disease: cellular and molecular mechanisms of disease-linked variants. Cell. Mol. Life Sci. *81*, 223. https://doi.org/10.1007/s00018-024-05262-8.
24. Zhang, F., Wu, Z., Long, F., Tan, J., Gong, N., Li, X., and Lin, C. (2022). The Roles of ATP13A2 Gene Mutations Leading to Abnormal Aggregation of alpha-Synuclein in Parkinson's Disease. Front. Cell. Neurosci. *16*, 927682. https://doi.org/10.3389/fncel.2022.927682.
25. Je, G., Guhathakurta, S., Yun, S.P., Ko, H.S., and Kim, Y.S. (2018). A novel extended form of alpha-synuclein 3′UTR in the human brain. Mol. Brain *11*, 29. https://doi.org/10.1186/s13041-018-0371-x.
26. Zhang, M., Chen, D., Xia, J., Han, W., Cui, X., Neuenkirchen, N., Hermes, G., Sestan, N., and Lin, H. (2017). Post-transcriptional regulation of mouse neurogenesis by Pumilio proteins. Genes Dev. *31*, 1354–1369. https://doi.org/10.1101/gad.298752.117.
27. Botta, S., de Prisco, N., Chemiakine, A., Brandt, V., Cabaj, M., Patel, P., Doron-Mandel, E., Treadway, C.J., Jovanovic, M., Brown, N.G., et al. (2023). Dosage sensitivity to Pumilio1 variants in the mouse brain reflects distinct molecular mechanisms. EMBO J. *42*, e112721. https://doi.org/10.15252/embj.2022112721.
28. Calabresi, P., Mechelli, A., Natale, G., Volpicelli-Daley, L., Di Lazzaro, G., and Ghiglieri, V. (2023). Alpha-synuclein in Parkinson's disease and other synucleinopathies: from overt neurodegeneration back to early synaptic dysfunction. Cell Death Dis. *14*, 176. https://doi.org/10.1038/s41419-023-05672-9.
29. Martinez, J.C., Randolph, L.K., Iascone, D.M., Pernice, H.F., Polleux, F., and Hengst, U. (2019). Pum2 Shapes the Transcriptome in Developing Axons through Retention of Target mRNAs in the Cell Body. Neuron *104*, 931–946 e935. https://doi.org/10.1016/j.neuron.2019.08.035.
30. Hallacli, E., Kayatekin, C., Nazeen, S., Wang, X.H., Sheinkopf, Z., Sathyakumar, S., Sarkar, S., Jiang, X., Dong, X., Di Maio, R., et al. (2022). The Parkinson's disease protein alpha-synuclein is a modulator of processing bodies and mRNA stability. Cell *185*, 2035–2056.e33. https://doi.org/10.1016/j.cell.2022.05.008.
31. Lam, I., Ndayisaba, A., Lewis, A.J., Fu, Y., Sagredo, G.T., Kuzkina, A., Zaccagnini, L., Celikag, M., Sandoe, J., Sanz, R.L., et al. (2024). Rapid iPSC inclusionopathy models shed light on formation, consequence, and molecular subtype of alpha-synuclein inclusions. Neuron *112*, 2886–2909.e16. https://doi.org/10.1016/j.neuron.2024.06.002.
32. Ferreira, A., and Caceres, A. (1992). Expression of the class III beta-tubulin isotype in developing neurons in culture. J. Neurosci. Res. *32*, 516–529. https://doi.org/10.1002/jnr.490320407.
33. Chambers, S.M., Fasano, C.A., Papapetrou, E.P., Tomishima, M., Sadelain, M., and Studer, L. (2009). Highly efficient neural conversion of human ES and iPS cells by dual inhibition of SMAD signaling. Nat. Biotechnol. *27*, 275–280. https://doi.org/10.1038/nbt.1529.
34. Vierbuchen, T., Ostermeier, A., Pang, Z.P., Kokubu, Y., Südhof, T.C., and Wernig, M. (2010). Direct conversion of fibroblasts to functional neurons by defined factors. Nature *463*, 1035–1041. https://doi.org/10.1038/nature08797.
35. Kamath, T., Abdulraouf, A., Burris, S.J., Langlieb, J., Gazestani, V., Nadaf, N.M., Balderrama, K., Vanderburg, C., and Macosko, E.Z. (2022). Single-cell genomic profiling of human dopamine neurons identifies a population that selectively degenerates in Parkinson's disease. Nat. Neurosci. *25*, 588–595. https://doi.org/10.1038/s41593-022-01061-1.

36. Morabito, S., Reese, F., Rahimzadeh, N., Miyoshi, E., and Swarup, V. (2023). hdWGCNA identifies co-expression networks in high-dimensional transcriptomics data. Cell Rep. Methods *3*, 100498. https://doi.org/10.1016/j.crmeth.2023.100498.

37. Gouveia Roque, C., Phatnani, H., and Hengst, U. (2024). The broken Alzheimer's disease genome. Cell Genom. *4*, 100555. https://doi.org/10.1016/j.xgen.2024.100555.

38. Rudakou, U., Yu, E., Krohn, L., Ruskey, J.A., Asayesh, F., Dauvilliers, Y., Spiegelman, D., Greenbaum, L., Fahn, S., Waters, C.H., et al. (2021). Targeted sequencing of Parkinson's disease loci genes highlights SYT11, FGF20 and other associations. Brain *144*, 462–472. https://doi.org/10.1093/brain/awaa401.

39. Tagliafierro, L., Glenn, O.C., Zamora, M.E., Beach, T.G., Woltjer, R.L., Lutz, M.W., and Chiba-Falek, O. (2017). Genetic analysis of alpha-synuclein 3′ untranslated region and its corresponding microRNAs in relation to Parkinson's disease compared to dementia with Lewy bodies. Alzheimer's Dement. *13*, 1237–1250. https://doi.org/10.1016/j.jalz.2017.03.001.

40. Tseng, E., Rowell, W.J., Glenn, O.C., Hon, T., Barrera, J., Kujawa, S., and Chiba-Falek, O. (2019). The Landscape of SNCA Transcripts Across Synucleinopathies: New Insights From Long Reads Sequencing Analysis. Front. Genet. *10*, 584. https://doi.org/10.3389/fgene.2019.00584.

41. Adamowicz, D.H., Roy, S., Salmon, D.P., Galasko, D.R., Hansen, L.A., Masliah, E., and Gage, F.H. (2017). Hippocampal alpha-Synuclein in Dementia with Lewy Bodies Contributes to Memory Impairment and Is Consistent with Spread of Pathology. J. Neurosci. *37*, 1675–1684. https://doi.org/10.1523/JNEUROSCI.3047-16.2016.

42. Otero-Jimenez, M., Wojewska, M.J., Binding, L.P., Jogaudaite, S., Gray-Rodriguez, S., Young, A.L., Gentleman, S., and Alegre-Abarrategui, J. (2025). Neuropathological stages of neuronal, astrocytic and oligodendrocytic alpha-synuclein pathology in Parkinson's disease. Acta Neuropathol. Commun. *13*, 25. https://doi.org/10.1186/s40478-025-01944-x.

43. Baleriola, J., Walker, C.A., Jean, Y.Y., Crary, J.F., Troy, C.M., Nagy, P.L., and Hengst, U. (2014). Axonally synthesized ATF4 transmits a neurodegenerative signal across brain regions. Cell *158*, 1159–1172. https://doi.org/10.1016/j.cell.2014.07.001.

44. Loedige, I., Baranovskii, A., Mendonsa, S., Dantsuji, S., Popitsch, N., Breimann, L., Zerna, N., Cherepanov, V., Milek, M., Ameres, S., and Chekulaeva, M. (2023). mRNA stability and m(6)A are major determinants of subcellular mRNA localization in neurons. Mol. Cell *83*, 2709–2725.e10. https://doi.org/10.1016/j.molcel.2023.06.021.

45. Pieger, K., Schmitt, V., Gauer, C., Gießl, N., Prots, I., Winner, B., Winkler, J., Brandstätter, J.H., and Xiang, W. (2022). Translocation of Distinct Alpha Synuclein Species from the Nucleus to Neuronal Processes during Neuronal Differentiation. Biomolecules *12*, 1108. https://doi.org/10.3390/biom12081108.

46. Seebauer, L., Schneider, Y., Drobny, A., Plötz, S., Koudelka, T., Tholey, A., Prots, I., Winner, B., Zunke, F., Winkler, J., and Xiang, W. (2022). Interaction of Alpha Synuclein and Microtubule Organization Is Linked to Impaired Neuritic Integrity in Parkinson's Patient-Derived Neuronal Cells. Int. J. Mol. Sci. *23*, 1812. https://doi.org/10.3390/ijms23031812.

47. Nicolas, G., Wallon, D., Goupil, C., Richard, A.C., Pottier, C., Dorval, V., Sarov-Rivière, M., Riant, F., Hervé, D., Amouyel, P., et al. (2016). Mutation in the 3′ untranslated region of APP as a genetic determinant of cerebral amyloid angiopathy. Eur. J. Hum. Genet. *24*, 92–98. https://doi.org/10.1038/ejhg.2015.61.

48. Shaheen, N., Shaheen, A., Osama, M., Nashwan, A.J., Bharmauria, V., and Flouty, O. (2024). MicroRNAs regulation in Parkinson's disease, and their potential role as diagnostic and therapeutic targets. npj Parkinson's Dis. *10*, 186. https://doi.org/10.1038/s41531-024-00791-2.

49. Yaylaoglu, M.B., Titmus, A., Visel, A., Alvarez-Bolado, G., Thaller, C., and Eichele, G. (2005). Comprehensive expression atlas of fibroblast growth factors and their receptors generated by a novel robotic in situ hybridization platform. Dev. Dyn. *234*, 371–386. https://doi.org/10.1002/dvdy.20441.

50. Carson, J.P., Eichele, G., and Chiu, W. (2005). A method for automated detection of gene expression required for the establishment of a digital transcriptome-wide gene expression atlas. J. Microsc. *217*, 275–281. https://doi.org/10.1111/j.1365-2818.2005.01450.x.

51. Hao, Y., Stuart, T., Kowalski, M.H., Choudhary, S., Hoffman, P., Hartman, A., Srivastava, A., Molla, G., Madad, S., Fernandez-Granda, C., and Satija, R. (2024). Dictionary learning for integrative, multimodal and scalable single-cell analysis. Nat. Biotechnol. *42*, 293–304. https://doi.org/10.1038/s41587-023-01767-y.

52. Lee, W., de Prisco, N., and Gennarino, V.A. (2022). Identifying patients and assessing variant pathogenicity for an autosomal dominant disease-driving gene. STAR Protoc. *3*, 101150. https://doi.org/10.1016/j.xpro.2022.101150.

53. Chen, D., Zheng, W., Lin, A., Uyhazi, K., Zhao, H., and Lin, H. (2012). Pumilio 1 suppresses multiple activators of p53 to safeguard spermatogenesis. Curr. Biol. *22*, 420–425. https://doi.org/10.1016/j.cub.2012.01.039.

54. Byers, B., Cord, B., Nguyen, H.N., Schüle, B., Fenno, L., Lee, P.C., Deisseroth, K., Langston, J.W., Pera, R.R., and Palmer, T.D. (2011). SNCA triplication Parkinson's patient's iPSC-derived DA neurons accumulate alpha-synuclein and are susceptible to oxidative stress. PLoS One *6*, e26159. https://doi.org/10.1371/journal.pone.0026159.

55. Chung, C.Y., Khurana, V., Auluck, P.K., Tardiff, D.F., Mazzulli, J.R., Soldner, F., Baru, V., Lou, Y., Freyzon, Y., Cho, S., et al. (2013). Identification and rescue of alpha-synuclein toxicity in Parkinson patient-derived neurons. Science *342*, 983–987. https://doi.org/10.1126/science.1245296.

56. Lee, S., Kopp, F., Chang, T.C., Sataluri, A., Chen, B., Sivakumar, S., Yu, H., Xie, Y., and Mendell, J.T. (2016). Noncoding RNA NORAD Regulates Genomic Stability by Sequestering PUMILIO Proteins. Cell *164*, 69–80. https://doi.org/10.1016/j.cell.2015.12.017.

57. Mazzara, P.G., Muggeo, S., Luoni, M., Massimino, L., Zaghi, M., Valverde, P.T.T., Brusco, S., Marzi, M.J., Palma, C., Colasante, G., et al. (2020). Frataxin gene editing rescues Friedreich's ataxia pathology in dorsal root ganglia organoid-derived sensory neurons. Nat. Commun. *11*, 4178. https://doi.org/10.1038/s41467-020-17954-3.

58. de Prisco, N., Botta, S., Lee, W., Rezazadeh, S., Chemiakine, A., and Gennarino, V.A. (2022). Determining the effects of loss of function mutations in human cell lines. STAR Protoc. *3*, 101232. https://doi.org/10.1016/j.xpro.2022.101232.

59. Servadio, A., Koshy, B., Armstrong, D., Antalffy, B., Orr, H.T., and Zoghbi, H.Y. (1995). Expression analysis of the ataxin-1 protein in tissues from normal and spinocerebellar ataxia type 1 individuals. Nat. Genet. *10*, 94–98. https://doi.org/10.1038/ng0595-94.

60. Park, J.W., Vahidi, B., Taylor, A.M., Rhee, S.W., and Jeon, N.L. (2006). Microfluidic culture platform for neuroscience research. Nat. Protoc. *1*, 2128–2136. https://doi.org/10.1038/nprot.2006.316.

61. Taylor, A.M., Blurton-Jones, M., Rhee, S.W., Cribbs, D.H., Cotman, C.W., and Jeon, N.L. (2005). A microfluidic culture platform for CNS axonal injury, regeneration and transport. Nat. Methods *2*, 599–605. https://doi.org/10.1038/nmeth777.

62. Pfaffl, M.W. (2001). A new mathematical model for relative quantification in real-time RT-PCR. Nucleic Acids Res. *29*, e45.

STAR★METHODS

KEY RESOURCES TABLE

REAGENT or RESOURCE	SOURCE	IDENTIFIER
Antibodies		
Mouse neuron-specific beta-III Tubulin antibody	R and D Systems	Cat# MAB1195 RRID: AB_357520
Rabbit anti-Pumilio 1 antibody	Abcam	Cat# ab92545 RRID:AB_10563695
Anti-Synuclein, alpha	Millipore	Cat# AB5038 RRID:AB_91648
Goat anti-Pumilio 1, Affinity Purified	Bethyl	Cat# A300-201A RRID:AB_2253218
Rabbit Anti-Argonaute 2 Monoclonal	Cell Signaling Technology	Cat# 2897 RRID:AB_2096291
Recombinant Anti-Alpha-synuclein	Abcam	Cat# ab212184 RRID:AB_2941889
Mouse Anti-Rabbit GADPH Monoclonal	Millipore	Cat# CB1001 RRID:AB_2107426
alpha Tubulin	Abcam	Cat# ab24246 RRID:AB_447954
Ataxin 1 - 11750	Huda Zoghbi Lab; Baylor College of Medicine	Cat# ATXN1-11750 RRID:AB_2721278
Rabbit control IgG (Purified Rabbit IgG)	Bethyl	Cat# P120-201 RRID:AB_479830
Mouse neuron-specific anti-beta-III Tubulin	Abcam	Cat# ab7751 RRID:AB_306045
Chemicals, peptides, and recombinant proteins		
Dulbecco's Modified Eagle Medium (DMEM)	Thermo Fisher Scientific	N/A
Fetal Bovine Serum		N/A
Matrigel in StemFlex Medium	Thermo Fisher Scientific	Cat# A3349401
mTeSR™Plus	StemCell Technologies	Cat# 100-1130
DMEM-F12	Thermo Fisher Scientific	Cat# 12634010
Neurobasal-A	Thermo Fisher Scientific	Cat# 10-888-022
MEM Non-Essential Amino Acids Solution (100X)	Thermo Fisher Scientific	Cat# 11140050
Penicillin-Streptomycin	Millipore Sigma	Cat# P4333
β-mercaptoethanol	Thermo Fisher Scientific	Cat# 31350010
Doxycycline	Millipore Sigma	Cat# D9891-5G
Glutamax	Thermo Fisher Scientific	Cat# 35050-061
N2	Thermo Fisher Scientific	Cat# 17502-048
B27 without Vitamin A	Gibco	Cat# 12587-010
Geltrex	Thermo Fisher Scientific	Cat# A1413202
Brain Derived Neurotrophic Factor	Gibco	Cat# 450-02-50UG
Adenosine-3′,5′-cyclic monophosphate	Millipore Sigma	Cat# 28745-100MG
L-Ascorbic Acid	Millipore Sigma	Cat# A92902-25G
Glial-Derived Neurotrophic Factor	Peprotech	Cat# 450-10-50
B27 without Vitamin A	Gibco	Cat# 12587-010
jetPRIME Transfection Reagent	Genesee	Cat# 55-133
PBS		N/A
Triton X-100	Fisher Scientific	Cat# BP151500

(*Continued on next page*)

Continued

REAGENT or RESOURCE	SOURCE	IDENTIFIER
Paraformaldehyde (PFA)	Fisher Scientific	Cat# F75P1GAL
Paraformaldehyde (PFA) for RNAscope	Fisher Scientific	Cat# AAJ19943K2
Donkey serum	Millipore Sigma	Cat# D9663-10ML
Platinum Taq DNA Polymerase High Fidelity	Invitrogen	N/A
pcDNA3.1(+)	Invitrogen	N/A
iScript Reverse Transcription Supermix	Bio-Rad Laboratories	Cat# 1708841BUN
PowerUp SYBR Green Master Mix	Applied Biosystem (Thermofisher)	Cat# A25778
Tris-HCl	Boston BioProducts	Cat#BM-324
NaCl	Fisher Scientific	Cat# BP358-10
NP-40	Thermofisher	Cat# 85214
Sodium deoxycholate	Fisher Scientific	Cat# AAJ6228822
Hydrogen peroxide	Advanced Cell Diagnostics	Cat# 323110
Target retrieval reagent	Advanced Cell Diagnostics	Cat# 322000
Protease digestion, Protease III	Advanced Cell Diagnostics	Cat# 322337
Opal 520 for Snca	Akoya Biosciences	Cat# OP-001001
Opal 570 for Th	Akoya Biosciences	Cat# OP-001003
TSA buffer	Advanced Cell Diagnostics	Cat# 322810
RNAscope washing buffer	Advanced Cell Diagnostics	Cat# 310091
Fluoro-Gel II with DAPI	Electron Microscopy Sciences	Cat# 1798551
SDS (20% SDM Dodecyl Sulfate (SDS))	Fisher Scientific	Cat# BP13111
Protease inhibitor cocktail (Xpert Protease Inhibitor Cocktail Solution(100X))	GenDEPOT	Cat# P3100-020
Phosphatase inhibitor cocktail (Xpert Phosphatase Inhibitor Cocktail Solution(100X))	GenDEPOT	Cat# P3200-020
Lipofectamine 2000 (Invitrogen™ Lipofectamine™ LTX Reagent with PLUS™ Reagent)	Fisher Scientific	Cat# 15-338-100
Lipofectamine 3000 Transfection Reagent	Fisher Scientific	Cat# L3000015
Dual Luciferase Reporter Assay System	Promega	N/A
RNase OUT (Invitrogen™ RNaseOUT™ Recombinant Ribonuclease Inhibitor)	Invitrogen (Fisher Scientific)	Cat# 10777019
Sepharose™ Protein A	Rockland	Cat# PA50-00-0002
yeast tRNA	Invitrogen (Fisher Scientific)	Cat# AM7119
qPCR Lentivirus Titer Kit	Applied Biological Materials	Cat# LV900
RNase-free DNase (RNase-Free DNase Set (50))	Roche (Qiagen)	Cat# 79254
Proteinase K	Roche (Fisher Scientific)	Cat# BP1700 500
Lenti-X™ Concentrator	Takara Bio	Cat# 631232
Penicillin-Streptomycin	Millipore Sigma	Cat# P4333
Critical commercial assays		
miRNeasy kit	Qiagen	Cat# 217004
Pierce BCA Protein Assay Kit	Fisher Scientific	Cat# PI23225
RNAscope Multiplex Fluorescent Detection Kit v2	Advanced Cell Diagnostics	Cat# 323110
4-12% NuPage Bis-Tris Gel	Invitrogen (Fisher Scientific)	Cat# NP0335BOX
QuikChange XL Site-Directed Mutagenesis kit (QuikChange II XL Site-Directed Mutagenesis Kit)	Stratagene (Agilent)	Cat# 200521
Coated glass slides	Probe On Plus Fisher Brand, Fisher Scientific	Cat# 22-037-246
Deposited data		
Raw Data	Mendeley	Link: https://data.mendeley.com/datasets/4km8t9w7jy/1

(*Continued on next page*)

Continued

REAGENT or RESOURCE	SOURCE	IDENTIFIER
Experimental models: Cell lines		
HEK293T	This paper	This paper
HCT116 WT	Joshua Mendell Lab	Joshua Mendell Lab
HCT116 Pum1-KO	Joshua Mendell Lab	Joshua Mendell Lab
SNCA triplication fibroblasts	Vikram Khurana Lab	Vikram Khurana Lab
Control fibroblasts	Vikram Khurana Lab	Vikram Khurana Lab
Lenti-X^{TM} 293T cell Line	Takara Bio	Cat# 632180
Experimental models: Organisms/strains		
Pum1 C57BL/6J	Haifan Lin Lab	This paper
Oligonucleotides		
Silencer Pre-designed siRNA for *PUM1*	Applied Biosystem	Assay ID s18681 Cat# 4392420
Silencer Pre-designed siRNA for *EIF2C2* (*AGO2*)	Applied Biosystem	Assay ID s25930 Cat# 4392420
Silencer Select Negative Control No. 2	Thermo Fisher Scientific	Cat# 4390847
miRIDIAN miRNA has-miR-7 mimic	Dharmacon	C-300518-07-005
miRIDIAN miRNA cel-miR-67 mimic negative control #1	Dharmacon	CN-001000-01-50
cDNA of *PUM1* (4635nt)	This paper	This paper
cDNA of *PUM2* (3195nt)	This paper	This paper
Taqman gene expression assay *Pum1* (Assay ID: Rn00569821_m1	Thermo Fisher Scientific	Cat# 4351372
Taqman gene expression assay *Snca* (Assay ID: Rn00569821_m1	Thermo Fisher Scientific	Cat# 4331182
Taqman gene expression assay *Rpl13* (Assay ID: Rn00821258_g1	Thermo Fisher Scientific	Cat# 4331182
Taqman probes gene expression assays *Pum1* (Assay ID: Rn01180594_m1)	Thermo Fisher Scientific	Cat# 4331182
Taqman probes gene expression assays *Snca* (Assay ID: Rn01425140_m1)	Thermo Fisher Scientific	Cat# 4331182
Taqman probes gene expression assays *Rps19* (Assay ID: Rn01458091_g1)	Thermo Fisher Scientific	Cat# 4331182
Tyrosine hydroxylase (TH) RNAscope probe	Advanced Cell Diagnostics	Cat# 317621-C2
SNCA RNAscope probe	Advanced Cell Diagnostics	Cat# 313281
See Table S4 for Primer sequences	This paper	This paper
Recombinant DNA		
Tet-On *PUM1*	This paper	This paper
psiCHECK-2 vector	This paper	This paper
pZIP-hUbC-eGFP-shControl (shCtrl)	Hengst Lab	Hengst Lab
pZIP-hUbC-eGFP-shPum1 (shPum1)	Hengst Lab	Hengst Lab
FUGW-hUbC-Pum1 (Pum1 OE)	Hengst Lab	Hengst Lab
pRP[Exp]-EGFP-EF1A>[myc-Pum1(P1021L)]	This paper	This paper
pRP[Exp]-EGFP-EF1A>[myc-Pum1(P760L)]	This paper	This paper
pRP[Exp]-EGFP-EF1A>[myc-Pum1(WT)]	This paper	This paper
pCMV ΔR8.9	David Baltimore Lab	David Baltimore Lab
pHCMV VSVg	David Baltimore Lab	David Baltimore Lab
FUGW	David Baltimore Lab	David Baltimore Lab
Software and algorithms		
GIMP	version 2.10.38	version 2.10.38
Seurat package	https://satijalab.org/seurat/	version 5.0.1

(*Continued on next page*)

Continued

REAGENT or RESOURCE	SOURCE	IDENTIFIER
R	https://www.r-project.org/	version 4.3.1
hdWGCNA package	https://smorabit.github.io/hdWGCNA/	version 0.3.03
GraphPad Prism 10	Version 10.2.1	Version 10.2.1
Microsoft Excel for Mac	N/A	N/A

EXPERIMENTAL MODEL AND STUDY PARTICIPANT DETAILS

RNA-cross linking immunoprecipitation (CLIP)

Brains from wild-type and *Pum1* knockout mice were extracted and processed for CLIP following the protocol previously described.[15] In brief, brain tissue was triturated in 8 mL of ice-cold HBSS until cell dissociation was homogeneous. The resulting suspension was transferred to a 10 cm sterile tissue culture plate and exposed to 150 mJ/cm^2 UVC (Stratagene, UV Stratalinker 2400) on ice. After this initial exposure, the suspension was gently swirled and exposed again to UVC at 100 mJ/cm^2. Cells were then pelleted for individual immunoprecipitation (IP) steps. Cell lysis was performed using a lysis buffer composed of 50 mM Tris-HCl (pH 7.4), 100 mM NaCl, 1% NP-40, 0.1% SDS, 0.5% sodium deoxycholate, 80 U/mL RNase OUT (Invitrogen), and protease inhibitors (GenDEPOT). The soluble fractions were pre-cleared with Protein A-Sepharose beads, rabbit control IgG (Sigma), 0.05% BSA, and 0.2 μg/mL yeast tRNA (Invitrogen). For immunoprecipitation, the lysates were incubated overnight at 4°C with 5 μg of either control IgG or Pum1 antibody (Bethyl Laboratories) together with Protein A-Sepharose beads on a rotating platform. The next day, the beads were washed five times with lysis buffer, followed by a 15-min treatment with 20 units of RNase-free DNase (Roche) at room temperature. Subsequently, the beads were treated with 50 μg of proteinase K (Roche) for 30 min at 37°C. The immunoprecipitated RNA was then extracted using the miRNeasy kit (Qiagen). RT-PCR was performed using two pairs of primers (region 1 and 2 in Figure S1D) specific for *Snca* cDNA regions upstream of the predicted PRE (see Table S4). A fraction (10%) of the pre-cleared lysate was used as the input control for RNA isolation.

In situ hybridization and analysis

Painted ISH was conducted following the method outlined by Gennarino et al.[15] In short, mice were anesthetized with isoflurane, and their brains were rapidly removed, immersed in OCT compound, and immediately flash-frozen by submerging the tissue molds in liquid nitrogen. Sagittal brain sections, 25 micrometers thick, were cut and mounted onto electrostatically coated glass slides (Probe On Plus Fisher Brand, Fisher Scientific). The sections were probed with *Pum1* and *Snca* mRNA probes using an automated *in situ* hybridization (ISH) protocol as previously described.[49] The probes were generated from reverse-transcribed mouse cDNA, amplified by Platinum Taq DNA Polymerase High Fidelity (Invitrogen) (see Table S4 for details). Three sagittal sections from three different mice per genotype were examined for each gene. Tissue preparation and the automated ISH process followed the protocols as previously described.[49,50]

The number of pixels in each channel—yellow, blue, and red—was counted using the free, open-source image editor GIMP, version 2.10.38 (https://www.gimp.org/). For whole-brain analysis, pixel counts were combined from two biological replicates, totaling 28 sagittal slices (covering the entire brain) for each genotype (1 male and 1 female) per gene, *Pum1* and *Snca*. For specific brain regions, the median sections—chosen to clearly display the entire brain region—were analyzed, totaling 8 sagittal sections for each genotype and gene. The analysis was performed in a blinded fashion without prior knowledge of the gene being analyzed. The total pixel counts were normalized against wild-type mice for statistical analysis (see Figures 3A, S2, S3C, and S4 legends).

RNAscope

To quantify *Snca* mRNA levels in individual neurons within the substantia nigra pars compacta (SNpc) of *Pum1*-Het, -KO, and wild-type (WT) mice (3 weeks old, $n = 3$ per genotype), fluorescence *in situ* hybridization (FISH) was performed using the RNAscope Multiplex Fluorescent Detection Kit v2 (Advanced Cell Diagnostics) according to the manufacturer's instructions. Dopaminergic neurons in the SNpc were identified using the tyrosine hydroxylase (*Th*) RNAscope probe (Advanced Cell Diagnostics, #317621-C2), and *Snca* mRNA transcripts were detected using the *Snca* RNAscope probe (Advanced Cell Diagnostics, #313281). Mice were perfused with 4% paraformaldehyde (PFA; Fisher Scientific, #AAJ19943K2) in PBS, and brains were post-fixed overnight in 4% PFA at 4°C. Coronal sections (100 μm thick) were cut using a vibratome (Leica VT1000s) from bregma −2.5 to −3.5 mm. After washing in PBS, sections were post-fixed in 4% PFA for 1 h, followed by treatment with hydrogen peroxide (Advanced Cell Diagnostics), target retrieval reagent (Advanced Cell Diagnostics), and protease digestion (Protease III, Advanced Cell Diagnostics). *Snca* and *Th* RNAscope probes were hybridized for 2 h. Signal amplification was performed using HRP, followed by fluorescent labeling with Opal 520 (Akoya Biosciences, #OP-001001) for *Snca* and Opal 570 (Akoya Biosciences, #OP-001003) for *Th*. Fluorescent dyes were diluted 1:1000 in TSA buffer (Advanced Cell Diagnostics). Between steps, sections were washed with RNAscope washing buffer (Advanced Cell Diagnostics) as instructed. Brain sections were mounted using Fluoro-Gel II with DAPI (Electron Microscopy Sciences, #1798551). Images were acquired using a Zeiss LSM 810 confocal microscope: whole-brain images were captured using a 10× objective with tile

scanning, and high-resolution images of individual SNpc neurons were captured with a 40× objective and z stack acquisition. z stack images were deconvolved using IMARIS 10 (Oxford Instruments) to improve clarity. The Extended Depth of Field (EDF) plugin (Biomedical Imaging Group) in ImageJ (FIJI) was used to merge Z-stacks into a single in-focus image. For *Snca* mRNA quantification, *Th*-positive, non-overlapping neurons in the SNpc were selected, and fluorescent particles within their somata were counted. Regions of interest (ROIs) were manually drawn in ImageJ (FIJI). Background noise was reduced using thresholding, and overlapping signals were separated via watershed segmentation. The "Analyze Particles" tool in ImageJ was then used to count individual *Snca* mRNA molecules (each fluorescent particle representing one transcript).

Lentivirus preparation and neuronal transduction

Lenti-X 293T cells (Takara Bio, San Jose, CA) were transfected at 90–99% confluency with 7.5μg lentiviral expression plasmid, 5.25μg packaging plasmid (pCMV ΔR8.9), and 2.25μg envelope plasmid (pHCMV VSVg) in a 10-cm plate using the Lipofectamine 3000 kit (Thermo Fisher Scientific, Waltham, MA) according to the manufacturer's instructions. pCMV ΔR8.9, pHCMV VSVg, and FUGW plasmids were generous gifts from David Baltimore. 14–16 h post-transfection, plates were briefly washed with 6mL pre-warmed medium (10% fetal bovine serum, 2mM GlutaMAX, $100U^{-1}$ penicillin-streptomycin in DMEM with high glucose/pyruvate and no glutamine; Thermo Fisher Scientific, Waltham, MA) and then replaced with 6mL of fresh pre-warmed medium. 30–36 h after changing the medium, the viral supernatant was collected, centrifuged at 500xg for 10 min at room temperature, and then filtered through a 0.45μm polyethersulfone (PES) syringe filter (Thermo Fisher Scientific, Waltham, MA). Lentiviruses were concentrated using the Lenti-X Concentrator reagent (Takara Bio, San Jose, CA) following manufacturer's instructions. Concentrated lentiviruses were subsequently aliquoted into tubes and stored at −80°C until use. Viral titers were calculated using the qPCR Lentivius Titer Kit (Applied Biological Materials, Richmond, Canada) according to the manufacturer's instructions. On DIV1, primary cortical neurons were transduced at an MOI of 10 for shRNA knockdown or an MOI of 5 for Pum1 overexpression. Knockdown and overexpression were verified by Western blot for each virus batch.

Single nuclei RNA sequencing from patients

Data preprocessing and metacell construction

Single-cell RNA sequencing data from human dopaminergic neurons were acquired from Kamath et al. (GEO accession no. GSE178265)[35] and analyzed using the Seurat package (version 5.0.1) in R (version 4.3.1).[51] Data normalization was performed using the Normalize Data Seurat function with default parameters on the RNA assay. Variable features were identified using FindVariableFeatures, and data scaling was conducted with ScaleData. Principal component analysis (PCA) was performed using RunPCA with 20 principal components to reduce dimensionality. To reduce technical noise and sparsity in single-nuclei RNAseq data, metacells were constructed using the hdWGCNA package (version 0.3.03).[36] The dataset was prepared for weighted gene co-expression network analysis (WGCNA) using the SetupForWGCNA function, selecting genes expressed in at least 5% of cells (fraction = 0.05). Cell type annotations were assigned according to the clusters defined in the original source paper, and metacells were generated using MetacellsByGroups with parameters k = 25, max_shared = 5, mode = "average", and target_metacells = 1000. The resulting metacell object underwent normalization, variable feature identification, scaling, and PCA as described above using default parameters.

Correlation analysis and permutation testing

The normalized and scaled expression levels of two genes of interest were extracted from each metacell and analyzed for correlation by calculating Spearman's rank coefficient, a non-parametric test given the unknown normality of any given gene's distribution. To assess the statistical significance of the observed correlation, a permutation test was conducted. The permutation test assesses the likelihood of observing the calculated correlation coefficient under the null hypothesis of no association, providing a non-parametric method to evaluate statistical significance without relying on distributional assumptions. The raw count data for one gene was randomly shuffled across cells without replacement. For each permutation, the shuffled counts were substituted back into the dataset, and the entire preprocessing and metacell construction pipeline and normalization was repeated using identical parameters. The correlation between our genes of interest was then recalculated for each permuted dataset using the same methods as above. A total of 100 permutations were performed for each comparison to create an empirical null distribution for our correlation statistic. The *p*-value was determined based on the rate of permutations with correlations at or more extreme than the original observed correlation (two-tailed). It is worth noting that a minor inherent correlation appears to be present when creating the empirical null distribution for any two genes, likely due to the normalization and scaling steps prior to the correlation calculations. Thus, the baseline null correlation used for calculating the number of extreme observations in any given distribution is centered around the empirically derived mean from permutation testing, rather than zero.

Search of clinical databases for individuals with PD carrying *PUM1* variants

We extracted all *PUM1* coding variants from the exomes and genomes of patients with PD (n = 3,484; 739 from Columbia and 2745 from AMP-PD). We filtered variants for those that are absent or very rare in control databases (e.g., gnomAD v.4.1, Columbia in-house databases, AMP-PD controls genomes). We used splice AI (https://spliceailookup.broadinstitute.org/) in May 2025 to extract predictors of protein functional disruptions and a combination of frequency in PD and rarity in controls, though we acknowledge that protein pathogenicity algorithms often do not agree with each other.[52]

Animals

All animal procedures were approved by the Institutional Animal Care and Use Committee at Columbia University, New York, under protocol AC-AAAU8490. Mice were kept on a 12-h light/dark cycle with regular chow and water available *ad libitum*. *Pum1* knockout mice were generated as previously described.[53] An equal number of males and females were used in all assays described in this manuscript. For brain dissection, mice were anesthetized with isoflurane, and the brains were rapidly removed from the skull and lysed in the appropriate buffer according to the experimental requirements.

METHOD DETAILS

Cell culture

We grew human HEK293T, HCT116, and SH-SY5Y cells in Dulbecco's Modified Eagle's Medium (DMEM, Invitrogen) fortified with 10% heat-inactivated Fetal Bovine Serum and treated with 1% penicillin/streptomycin. Cells were continually incubated at 37°C in a humidified chamber circulating 5% CO_2. Both patient-derived iPSCs and their respective isogenic controls were obtained from Vikram Khurana under the IRB protocol.[30,31] *SNCA* triplication fibroblasts obtained from a female Iowa kindred patient (age 55), a male Iowa kindred patient (age 48) was previously described.[30,31,54,55] Detailed protocols for iPSC generation and maintenance were also detailed previously.[30,31] Briefly, fibroblasts were reprogrammed to iPSC via mRNA-based methods. iPSCs were maintained on Matrigel in StemFlex Medium (Thermo Fisher Scientific). Isogenic *SNCA* knock-down controls were generated via CRISPR-Cas9 mediated gene editing. Levels of α-Syn were assessed across the isogenic series (4-copy, 2-copy) by western blot.

Human Tet-On *NGN2* iPSCs were generated with all-in-one PiggyBac plasmid[30,31] to ensure robust and efficient neuronal differentiation and were maintained in feeder-free conditions in a mTeSRPlus (StemCell Technologies) medium supplemented with 1% Penicillin-Streptomycin (Millipore Sigma). Cells were grown and maintained in 6-well culture plates coated with Geltrex (Thermo Fisher Scientific). On DIV0 50.000 iPSCs/cm2 were seeded in mTeSR with Y27632 100 μM. The following day (DIV1), KSR medium was added (DMEM-F12 with 15% KSR, 1% of each: pen/strep; Non-Essential Amino Acids (NEAA, Thermo Fisher Scientific) with β-mercaptoethanol (100 μM, Thermo Fisher Scientific) and L-Glutamate (2 nM, Thermo Fisher Scientific). The following day (DIV 2) the KSR medium was supplemented with doxycycline (dox 2 mg/mL; Millipore Sigma) and gradually switched to N2/B27 Media (Neurobasal A medium (Thermo Fisher Scientific); N2 (Thermo Fisher Scientific); B27 without Vitamin A (Thermo Fisher Scientific); pen/strep; NEAA, and L-Glutamine)) by DIV4. The medium was subsequently changed every 48 h. On DIV7, recombinant human Brain Derived Neurotrophic Factor 10 ng/mL (BDNF, PeproTech); Glial-Derived Neurotrophic Factor 10 ng/mL (GDNF, PeproTech); Adenosine-3′,5′-cyclic monophosphate 250μM (dcAMP Peprotech) and Ascorbic Acid 200 μM (AA Merck), were added to the base medium. The medium was subsequently changed every 48 h. Induced Neurons were Tet-On *PUM1* infected (MOI3-5) on DIV14. In 16 to 20 h after infection, fresh medium was added. On DIV 15 dox was reduced to 1 mg/mL and maintained until DIV21. All cell lines used in this study were previously authenticated by short tandem repeat (STR) profiling and have been widely used and validated in prior publications.[27,30,31,56] The cell lines were routinely tested and confirmed to be free of mycoplasma contamination. See Figure S6A for schematic representation.

Cell transfection

For transfection, we used jetPRIME Transfection Reagent (Polyplus Transfection) according to the provided protocol. Cells were transfected with 50 pmol of Silencer Pre-designed siRNA for *PUM1* (Applied Biosystem). Silencer Pre-designed siRNA for *EIF2C2* (*AGO2*) (Applied Biosystem).[15] Silencer Select Negative Control No. 2 (Thermo Fisher Scientific). In overexpression experiments, the full cDNA of *PUM1* (4635nt) and *PUM2* (3195nt) was amplified using Platinum Taq DNA Polymerase High Fidelity (Invitrogen) before being cloned into a mammalian expression vector, pcDNA3.1(+) (Invitrogen). Cells were transfected with anywhere from 0.5μg to 2μg of either pcDNA3.1(+)-*PUM1* or pcDNA3.1(+)-*PUM2* or control pcDNA3.1(+). For miR-7 and Cel-miR-67 experiments, 50 pmol of the miRIDIAN Dharmacon microRNA mimics were transfected. miRIDIAN miRNA has-miR-7 mimic (Dharmacon). miRIDIAN miRNA cel-miR-67 mimic negative control #1 (Dharmacon).

For the patient variant assays, 70,000 cells were seeded into a 12-well plate and transfected at 60% confluency with one of three constructs: pRP[Exp]-EGFP-EF1A>[myc-Pum1(WT)], pRP[Exp]-EGFP-EF1A>[myc-Pum1(P1019L)] or pRP[Exp]-EGFP-EF1A>[myc-Pum1(P760L)]. After 48 h, cells were washed with PBS, then Trypsinized (1X), and collected before light centrifugation (500 RPM for 5 min at room temperature) for pelleting. The supernatant was removed, and the cell pellet collected for further processing.

Immunocytochemical assays

Immunocytochemical analyses were performed as described previously[57]: iNs were fixed for 20 min at room temperature in 4% paraformaldehyde in PBS, permeabilized for 30 min in PBS containing 0.1% Triton X-100 and 10% donkey serum and incubated overnight at 4°C in PBS containing 10% normal donkey serum and primary antibodies. Then cells were washed three times with PBS and incubated for 2 h at room temperature with secondary antibodies. iNs were stained against TUJ1 (R&D), PUM1 (Abcam), and α-synuclein (Millipore). Images for quantification were selected randomly. To quantify the immunopositively area (expressed in pixels) pictures in each coverslip/sample were taken and the area of interest was calculated using the ImageJ software.

RNA extraction and quantitative real-time PCR

For *in vitro* experiments, HEK293T, HCT116, and SH-SY5Y cells were seeded in six-well culture plates. After 48hrs post-transfection, we collected cells and used the miRNeasy kit (Qiagen) to extract total RNA according to manufacturer instructions.[58] Mice were sacrificed by cervical dislocation after anesthetization with isoflurane in a bell jar. One hemisphere was used for RNA extraction, while the other was used for protein extraction. Half-brains were placed in 1.4 mL of Qiazol Lysis Reagent and homogenized using syringe trituration of progressively narrower gauges (18G, 23G, and 26G), then left at room temperature for 5 min. Next, 280μL of chloroform was added to the mixture and vigorously shaken before being left at room temperature for 3 min. Homogenates were centrifugated at 12,000g at 4°C for 15 min for phase separation; the upper phase was collected and subsequently purified using miRNeasy kit (Qiagen) according to manufacturer instructions. Total RNA was quantified using NanoDrop 1000 (Thermo Fisher). 1μg of RNA was used for cDNA synthesis using iScript Reverse Transcription Supermix per manufacturer instructions (Bio-Rad Laboratories). Quantitative real-time polymerase chain reaction (PCR) experiments were performed using the CFX96 Touch Real-Time PCR Detection System (Bio-Rad Laboratories) with PowerUp SYBR Green Master Mix (Applied Biosystem). All qPCR analyses were done using the comparative Ct method by normalizing relative expression against the housekeeping gene *GAPDH*.

For rat neurons, primary rat cortical neurons were plated at a density of 750,000–800,000 cells/well in 6-well plates. Two wells were plated per condition and were subsequently pooled during collection. On DIV1, neurons were transduced with shCtrl, sh*Pum1*, or *Pum1* OE lentiviruses at a MOI of 5–10 and maintained until DIV8. On DIV8, cells were washed once with ice-cold HBSS and then lysed in 200 μL TRIzol Reagent per well (Thermo Fisher Scientific, Waltham, MA). Cells were immediately scraped with a cell scraper, collected in microcentrifuge tubes, incubated on ice for 5 min, and then centrifuged at 12,000xg for 5min at 4°C. Supernatant was transferred to a fresh microcentrifuge tube and mixed thoroughly with an equal volume of 100% ethanol. Total RNA was isolated using the Direct-zol RNA MicroPrep kit (Zymo Research, Irvine, CA) with DNase I treatment following the manufacturer's instructions. RNA was eluted in 15 μL DNase/RNase free H_2O and concentrations were obtained via NanoDrop. Samples were stored at −80°C until use. qPCR was performed using the Luna Universal Probe One-Step RT-qPCR kit (New England Biolabs, Ipswich, MA) according to manufacturer's instructions. 250ng of template RNA was used per well, and Taqman FAM probes were used for detection (Thermo Fisher Scientific, Waltham, MA). qPCR was run on the QuantStudio 3 Real-Time PCR System (Thermo Fisher Scientific, Waltham, MA), and therefore a 60s extension time was used per manufacturer's instructions. *Rpl13* was used here as housekeeping gene for normalization.

For quantification, cycle threshold (CT) values were averaged across duplicates for each condition to obtain the CT mean. Signal was normalized to the housekeeping gene by subtracting the CT mean obtained for the housekeeping gene from each target gene (ΔCT). Then, ΔΔCT was obtained by subtracting the control ΔCT value from the ΔCT value for each sample. To obtain the relative fold change of each gene, the formula $2^{-\Delta\Delta CT}$ was used. Changes in expression level were calculated using standard deviation of the ΔCt, or the ΔΔCt. One-sample t tests were performed for statistical analysis. See Table S4 for primers.

Protein extraction and western blot

HEK293T and HCT116 cells were seeded in six-well culture plates. After 48hrs post-transfection, we collected cells for lysis. Mice were sacrificed as described for RNA extraction. One hemisphere was used for lysis and protein extraction. RIPA buffer (25mM Tris-HCl, pH 7.6, 150mM NaCl, 1% NP-40, 1% sodium deoxycholate, 0.1% SDS, 1× protease inhibitor cocktail (GenDEPOT) and 1× phosphatase inhibitor cocktail (GenDEPOT) was used for lysis of cells and tissue alike, with volumes of 100μL or 1 mL, respectively. Cells were lysed using pipette trituration. Brain tissue was homogenized using syringe trituration of progressively narrower gauges (18G, 23G, and 26G). After lysis, samples were placed on ice for 15 min and then centrifugated at 13,000g at 4°C for 20 min. The upper phase was collected and triturated with a tighter needle gauge (28G). Samples were again placed on ice for 15 min and then centrifugated at 13,000g at 4°C for 20 min. Protein quantification was done using the Pierce BCA Protein Assay Kit (Thermo Fisher Scientific) and NanoDrop 1000 (Thermo Fisher Scientific). Proteins were resolved by high resolution 4–12% NuPage Bis-Tris Gel (Invitrogen) per manufacturer's instructions. The following antibodies were used for all Western blots and were commercially acquired or gifted by the Zoghbi lab at Baylor College of Medicine: goat anti-PUM1 (1:5000, Bethyl Laboratories); rabbit anti-AGO2 (1:1000, Cell Signaling Technology); rabbit anti α-synuclein (1:1000, Abcam); anti-GAPDH (1:10000, Millipore); rabbit anti-TUBA (1:10000); and rabbit anti-ATXN1 (1:2500).[59]

For the rat neurons, primary rat cortical neurons were plated at a density of 275,000 cells/well in 12-well plates. Two wells were plated per condition and were subsequently pooled during collection. On DIV1, neurons were transduced with shCtrl, sh*Pum1*, or *Pum1* OE lentiviruses at a MOI of 5–10 and maintained until DIV8. On DIV8, cells were washed once with ice-cold HBSS and then lysed in 80 μL 2X Laemmli sample buffer (Bio-Rad, Hercules, CA) containing 100mM dithiothreitol (DTT) per well (Thermo Fisher Scientific, Waltham, MA). Cells were scraped for 30s with a cell scraper and collected in chilled microcentrifuge tubes on ice. Samples were incubated at 95°C for 5 min, briefly centrifuged, and then stored at −20°C until use. SDS-PAGE was performed by loading 27 μL of samples into NuPAGE 4–12% bis-tris gels (Thermo Fisher Scientific, Waltham, MA). Gels were run in NuPAGE MOPS SDS running buffer (Thermo Fisher Scientific, Waltham, MA) at 60-65V for 15 min, and then the voltage was increased to 160-165V for approximately 1 h. Proteins were transferred to 0.45 μm nitrocellulose membranes for 90 min at 220mA in cold transfer buffer (25mM Tris, 192mM glycine, 20% methanol) using the Mini-PROTEAN Tetra Vertical Electrophoresis system (Bio-Rad, Hercules, CA). After transfer, membranes were briefly stained with Ponceau S solution to visualize total protein content, washed three times with TBS-T (0.1% Tween 20 in Tris-buffered saline) to completely remove the Ponceau S stain, and

then incubated for 1 h in blocking solution (2% bovine serum albumin in TBS-T) on a rocker at room temperature. Membranes were incubated overnight with primary antibodies on a rocker at 4°C. The next day, membranes were washed three times with TBS-T and then incubated for 1 h at room temperature on a rocker with HRP-conjugated secondary antibodies (Thermo Fisher Scientific, Waltham, MA), which were diluted 1:10,000 in TBS-T. After secondary antibody incubation, membranes were washed three times with TBS-T, and then subsequently developed using 1-Shot Digital ECL (Kindle Biosciences, Greenwich, CT) and imaged using the KwikQuant Imager (Kindle Biosciences, Greenwich, CT). The following antibodies were used for all Western blots: Rabbit anti-Pumilio1 (1:3000, Abcam); rabbit anti α-synuclein (1:1000, Abcam), and mouse anti-β-III-tubulin (1:10,000, Abcam).

For quantification, images were opened in Fiji as TIFFs, converted to 8-bit, and then inverted. The gel analyzer tool was used to draw a rectangular ROI around each band of interest, and then the intensity of each ROI was measured. The intensity of each band was determined by drawing a line across the bottom of each curve and then measuring the area under the curve. Intensity values for each band of interest were normalized by dividing the intensity of the housekeeping protein signal in the corresponding lane. Intensity values for each sample were then normalized to the control sample to obtain fold changes. One-sample t tests were performed for statistical analysis.

Luciferase assay

The full-length 3′ UTR of human *SNCA* mRNA was subcloned into psiCHECK-2 vector (Promega) by XbaI and NheI restriction enzymes. Mutagenesis to delete one or both PREs was performed using the QuikChange XL Site-Directed Mutagenesis kit (Stratagene). HEK293T cells in 24-well plates were transfected with 30 ng of psiCHECK-2 construct plus: 50 pmol of si*PUM1* or control scramble-siRNA and 0.5 μg of pcDNA3.1(+)-*PUM1* or control pcDNA3.1(+) using Lipofectamine 2000 (Invitrogen). After 24 h, luciferase activity was measured using the Dual Luciferase Reporter Assay System (Promega) according to the manufacturer's instructions.

Microfluidic chamber assay

Bipartite microfluidic chambers with a set of 750 μm-long microgroove channels were designed and produced in-house as previously described[29] using established protocols.[60,61] Rat primary hippocampal neurons were seeded in the somatic compartment of the chambers and infected on DIV0 with lentiviruses expressing sh*Pum1* or shControl shRNA constructs (transOMIC Technologies, Huntsville, AL) (shControl: tgctgttgacagtgagcgAAGGCAGAAGTATGCAAAGCATtagtgaagccacagatg taATGCTTTGCATACTTCTGCCTGtgcctactgcctcgga, sh*Pum1*: tgctgttgacagtgagcgcGGGATTGATGCAGACGTCAAAtagtgaagcc acagatgtaTTTGACGTCTGCATCAATCCCatgcctactgcctcgga; capital letters indicate gene-targeting region of hairpin). On DIV15, somatic and axonal compartment lysates were collected and pooled from 3 to 4 chambers for somatic lysate and 20–22 chambers for axonal lysate. RNA was extracted using Single Cell RNA Purification Kit (Norgen Biotech, Ontario, CA). After performing RT-PCR (iScript RT Supermix, Bio-Rad), axonal samples were pre-amplified (SsoAdvanced PreAmp Supermix, Bio-Rad) and qPCR was subsequently performed with SsoAdvanced Universal Probes Supermix (Bio-Rad) using Taqman probes gene expression assays (Thermo Fisher Scientific): *Pum1*: Rn01180594_m1, *Snca*: Rn01425140_m1, *Rps19*: Rn01458091_g1.

QUANTIFICATION AND STATISTICAL ANALYSIS

Experimental design

For protein and RNA quantification from cell lines, data were obtained from at least three independent experiments, each with three biological replicates. Throughout the study, the experimenter was blinded to the identity of control, treated, or untreated cell lines. In the mouse experiments, randomization and blinding were conducted as described above. The number of animals used, their sex, and the specific statistical tests applied are detailed in the figure legends. Sample size was determined based on prior experience with the same mouse model.[15]

Statistical analysis

Statistical analyses were performed using GraphPad Prism 10 (https://www.graphpad.com/scientific-software/prism/) and Microsoft Excel. All data are expressed as mean ± SEM. Detailed statistical information for each experiment is provided in the figures and their respective legends. Expression level ranges in qPCR were determined from at least three independent experiments, each with three biological replicates, by calculating the standard deviation of the ΔCt values.[62] Similarly, expression level ranges in western blot analyses were obtained from at least three independent experiments with three biological replicates. *p* values were determined using Student's t test or analysis of variance (ANOVA) with Tukey's post hoc test for multiple comparisons.